NAVAL POSTGRADUATE SCHOOL

MONTEREY, CALIFORNIA

THESIS

WIRELESS SENSOR NETWORK: CHANNEL PROPAGATION MEASUREMENTS AND COMPARISON WITH SIMULATION

by

Mohamad H. Alzaghal

June 2006

Thesis Advisor:	Weilian Su
Second Reader:	David Jenn

Approved for public release; distribution is unlimited

THIS PAGE INTENTIONALLY LEFT BLANK

REPORT DOCUMENTATION PAGE			Form Approved OMB No. 0704-0188
Public reporting burden for this collection of information is estimated to average 1 hour per response, including the time for reviewing instruction, searching existing data sources, gathering and maintaining the data needed, and completing and reviewing the collection of information. Send comments regarding this burden estimate or any other aspect of this collection of information, including suggestions for reducing this burden, to Washington headquarters Services, Directorate for Information Operations and Reports, 1215 Jefferson Davis Highway, Suite 1204, Arlington, VA 22202-4302, and to the Office of Management and Budget, Paperwork Reduction Project (0704-0188) Washington DC 20503.			
1. AGENCY USE ONLY ***(Leave blank)***	**2. REPORT DATE** June 2006	**3. REPORT TYPE AND DATES COVERED** Master's Thesis	
4. TITLE AND SUBTITLE: Wireless Sensor Network: Channel Propagation Measurements and Comparison with Simulation			**5. FUNDING NUMBERS**
6. AUTHOR(S) Mohamad H. Alzaghal			
7. PERFORMING ORGANIZATION NAME(S) AND ADDRESS(ES) Naval Postgraduate School Monterey, CA 93943-5000			**8. PERFORMING ORGANIZATION REPORT NUMBER**
9. SPONSORING / MONITORING AGENCY NAME(S) AND ADDRESS(ES) N/A			**10. SPONSORING / MONITORING AGENCY REPORT NUMBER**
11. SUPPLEMENTARY NOTES The views expressed in this thesis are those of the author and do not reflect the official policy or position of the Department of Defense or the U.S. Government.			
12a. DISTRIBUTION / AVAILABILITY STATEMENT Approved for public release; distribution is unlimited			**12b. DISTRIBUTION CODE**

13. ABSTRACT (maximum 200 words)

Wireless Sensor Networks (WSNs) is an important field of study as more and more applications are enhancing daily life. The technology trend is to achieve small-sized, cheap, and power efficient sensor nodes, which will make the system reliable and efficient. The Crossbow Technologies MICAz mote is an example used in this thesis. Measurements for its propagation characteristics in a realistic environment will help the deployment and installation of these motes to form a WSN. The CST Microwave Studio is used to build a simulation for the MICAz. The Rhino software is used to build Spanagel Hall, which is the location of the simulation.

All of these elements are integrated in Urbana. Urbana is a simulation tool used to simulate the propagation decay around the mote and investigate the irregularity of the electromagnetic field for the indoor environment of the motes. The results and comparisons between empirical and simulated data are intended for assisting in the design and future studies and deployment of WSNs in the real world.

14. SUBJECT TERMS Wireless Sensor Networks, Propagation Characteristics, MICAz Motes			**15. NUMBER OF PAGES** 83
			16. PRICE CODE
17. SECURITY CLASSIFICATION OF REPORT Unclassified	**18. SECURITY CLASSIFICATION OF THIS PAGE** Unclassified	**19. SECURITY CLASSIFICATION OF ABSTRACT** Unclassified	**20. LIMITATION OF ABSTRACT** UL

NSN 7540-01-280-5500 Standard Form 298 (Rev. 2-89)
Prescribed by ANSI Std. 239-18

THIS PAGE INTENTIONALLY LEFT BLANK

Approved for public release; distribution is unlimited

WIRELESS SENSOR NETWORK: CHANNEL PROPAGATION MEASUREMENTS AND COMPARISON WITH SIMULATION

Mohamad H. Alzaghal
Lieutenant Colonel, Jordanian Army
B.S., Mu'tah University, 1988

Submitted in partial fulfillment of the
requirements for the degree of

MASTER OF SCIENCE IN ELECTRICAL ENGINEERING

from the

NAVAL POSTGRADUATE SCHOOL
June 2006

Author: Mohamad H. Alzaghal

Approved by: Weilian Su
Thesis Advisor

David Jenn
Second Reader

Jeffrey Knorr
Chairman, Department of Electrical and Computer Engineering

THIS PAGE INTENTIONALLY LEFT BLANK

ABSTRACT

Wireless Sensor Networks (WSNs) is an important field of study as more and more applications are enhancing daily life. The technology trend is to achieve small-sized, cheap, and power efficient sensor nodes, which will make the system reliable and efficient. The Crossbow Technologies MICAz mote is an example used in this thesis. Measurements for its propagation characteristics in a realistic environment will help the deployment and installation of these motes to form a WSN. The CST Microwave Studio is used to build a simulation for the MICAz. The Rhino software is used to build Spanagel Hall, which is the location of the simulation.

All of these elements are integrated in Urbana. Urbana is a simulation tool used to simulate the propagation decay around the mote and investigate the irregularity of the electromagnetic field for the indoor environment of the motes. The results and comparisons between empirical and simulated data are intended for assisting in the design and future studies and deployment of WSNs in the real world.

THIS PAGE INTENTIONALLY LEFT BLANK

TABLE OF CONTENTS

LIST OF FIGURES

LIST OF TABLES

THIS PAGE INTENTIONALLY LEFT BLANK

ACKNOWLEDGMENTS

I would like to thank Professor Weilian Su, Professor David Jenn, and Mr. Bob Broadston for their help and guidance throughout this thesis work.

Also, I would like to thank my wife Nahla Alawadat and family for their understanding and constant support.

Last but not least, I wish to dedicate this work to the soul of my late father, Hisham Alzaghal, for all of his efforts throughout his life for his family.

THIS PAGE INTENTIONALLY LEFT BLANK

I. INTRODUCTION

A. BACKGROUND

The Wireless Sensor Network (WSN) technology is not a new concept; military applications have long been used for surveillance and data collection. A recent boost of interest in this technology and its applications results from the advance in the Micro-Electromechanical System (MEMS) making the fabrication of small-sized and cheap sensor nodes feasible.

Sensor nodes, or motes as many call them, are small-sized sophisticated sensors with the ability to be connected to each other. These motes could be deployed randomly using artillery or parachutes in the military domain. Another deployment method is to install the motes at specific location to get the best coverage and connectivity.

Sensor nodes are required to have many functions. Even though they are tiny, they should be able to sense the phenomenon (temperature, light, pressure, etc.), and at the same time to communicate with each other, to a base station, or to a cluster head.

Some applications require the WSN deployment to be widely spread, thus making its implementation more challenging. Sensor nodes should balance between the limited storage capacity and aggregation of data gathered to reduce congestion.

The assumption that the range of the sensor nodes is uniform and homogeneous does not echo the real behavior of the network with respect to power transmitted and received, which will affect the deployment and implementation of the WSN.

Although this study is focused on Crossbow Technologies MICAz sensor motes, many of the results are applicable to other platforms and systems and hopefully are useful for the design and implementation of the WSN.

B. OBJECTIVES

The objective of this thesis is to investigate the irregularity of the range and other propagation characteristics of the MICAz motes. This is primarily due to the complex

propagation environment in which the WSN operates. Testing and evaluation of these motes at the system-level were conducted. The results were analyzed and compared with simulations.

C. RELATED WORK

Recently, some research effort focused on the propagation modeling issues of WSNs. Part of the research is concentrated on the non-isotropic pattern phenomenon of the electromagnetic radiation field around the motes. Several authors [1,2,3,4,5] presented the problem and proposed solutions for it using empirical data and simulation techniques. They suggested the use of specific protocols and algorithm to cope with the non-uniform field measured around the motes.

In [1], Zhou, He, Krishnamurthy, and Stankovic discuss the impact of radio irregularity on the implementation of the WSN. They presented factors that create this phenomenon such as variance in the Radio Frequency (RF) transmitting power and different path losses of propagation. They established a radio model for simulation and called it the Radio Irregularity Model (RIM) to bridge the discrepancy between spherical radio models used by simulators and the physical reality of radio signals. They introduced six practical solutions for radio irregularity.

Radio channel models are presented in a general context in [3]. Zhon, Das, and Gupta evaluated and approximate radio coverage around the node. They measured the interference of the systems and introduced a "Disk Model" to approximate the radiation pattern, which is not always an accurate approximation.

Kotz, Newport, and Elliott [2] discussed the mistaken assumptions in wireless network research regarding the non-uniform field and asymmetric non-reciprocal field strength in both directions between the receiver and transmitter. The author focused on 802.11 wireless systems while this thesis will focus on 802.15 systems such as the WSN.

Other studies discussed the effect of transmission radius in wireless networks. In [6] and [7], Gupta and Kumar, Sanchez and Manzoni, respectively, analyzed the critical transmission range to maintain connectivity in wireless networks. In [6], Gupta and

Kumar presented a statistical analysis of the probability of connectivity and in [7] Sanchez and Manzoni provided a separate algorithm to establish this connectivity.

In the same area of work, Xue and Kumar [8], and Kleinrock and Silvester [9], analyzed the minimum number of neighbors that a node should have to maintain the network connection. In [10], Takagi and Kleinrock described a similar tradeoff for increasing the transmission radius: a shorter range implies less collisions and a longer range implies moving a packet further ahead in one hop. However, in that work, the authors wanted to maximize how fast a packet can reach its destination in point-to-point transmissions. The same tradeoff was studied by Royer, Melliar-Smith, and Moser [11].

Another important direction in the study of optimal transmission radius is targeted to improve network lifetime and energy consumption. In [12], Bahl, Wang, and Wattenhofer proposed a simple distributed algorithm, where each node can vary its transmission radius to increase network lifetime while maintaining connectivity. Xiao and Xu [13] investigated the effects of transmission radius in the energy efficiency of packet transmission. They also showed how some parameters of the physical layer model influence the performance of protocols at the network layer.

In [14], Stuedi, Chinellato, and Alonso have investigated connectivity in ad hoc networks under log-normal shadowing radio propagation. Their study targets networks with ACK-based media access, which requires symmetric links. In addition to the simulation results, the link probability as a function of nodes in the network, network size, average transmission radius, path loss exponent and shadowing deviation were derived.

In [4,5], Tingle and Swee, respectively, studied some aspects of the MICAz mote characteristics, which were measured and simulated. The antenna for the MICAz mote was studied thoroughly. In this thesis, a continuation of these measurements and simulations is considered with more exhaustive details and techniques. Although MICAz motes are used, this will be a baseline for other platforms to be studied.

Z´u˜niga and Krishnamachari in [15] addressed the problem of finding an optimal transmission radius for minimizing the settling time for flooding in sensor networks. This

problem merits discussion because flooding is still used in various wireless protocols. The authors proposed an analytical model verified by simulations that describes an optimal transmission radius for uniform and grid topologies.

In this thesis, the radiation pattern around the MICAz mote will be measured to show irregularity and other characteristics. The first phase is to measure baseline data for the mote in free space using an Anechoic Chamber. The second phase is to build the same environment in a simulator and compare the results with those obtained in the chamber.

The third phase is to measure the radiation pattern in the presence of multipath and interference. The fourth phase is to build the same multipath environment in a simulation and compare the results of the two.

An addition to the experimental setup and simulation is the examination of the effect of human presence. Another addition is the measurement of the effect of multiple motes transmitting at the same time. The results will help ascertain the nature of the irregularity and will help determine networking and deployment protocols algorithms for the WSNs.

D. THESIS ORGANIZATION

The thesis is divided into six chapters. Chapter II is an overview of wireless sensor networks: architecture and components. RF characteristics of sensor nodes and propagation models are presented in Chapter III. The experimental setup and simulation are described in Chapter IV. Lastly, conclusions and future work are presented in Chapter V.

II. OVERVIEW OF WIRELESS SENSOR NETWORKS

The growing number of applications of wireless sensor network (WSN) technology has stimulated the research in this field. The market is demanding such implementations especially in the military domain. WSN consists of sensor nodes (hundreds or maybe thousands) that sense certain phenomenon and these sensors are networked wirelessly to deliver the data to the user.

Many factors affect the design of the WSN. The designer should compromise depending on application, between node size, low power consumption, and other design objectives such as worldwide availability, network type, security requirements, cooperation/data aggregation, automatic self-organization, and data throughput. [16]

The communication technique should be bandwidth efficient and immune to channel changes such as fading and multipath. Processing capabilities should be distributed and not moved to the center station. Usually, some sort of identification (ID) is needed for routing data in a network, but the WSN should route data without a unique ID for each sensor, as they are numerous and the system cannot afford the overhead from such an ID.

Nodes should estimate their location to perform the required functions (as they are attached to a fixed place most of the time). It is not realistic to use GPS systems for many reasons, such as cost and size, not to mention that the GPS receiver must be in the line of sight (LOS) with the GPS satellites to measure the position.

A. WSN APPLICATIONS

There are many applications for the WSN in a wide variety of disciplines; the future for these applications is promising and not limited. These applications could be categorized as follows.

1. Inventory Applications

In the military domain, for example, the goal of Network Centric Operations (NCO) is to improve the decision-making process by providing the commanders with a clear image of the battlefield, and sensors are vital to this process. Sensors could be

attached to weapons and armaments, and could even be attached to the soldiers' accessories. Another example is in the health domain concerning the inventory of drugs or patient tracking.

2. Status Tracking Applications

In the agricultural domain example, farmers are able to monitor all circumstances about their product such as weather, plant growing, insecticides, fire control, flood detection, and the humidity level.

3. Control Applications

WSNs could be used as part of a control system for feedback to return a certain value for the phenomenon to be controlled. For example, in the health domain, the air around the patient could be controlled using such technology. Home automation is another example. WSNs are playing a vital role in automated appliances appearing in homes in the future.

4. Surveillance Applications

In traffic control, for example, roads and intersections could be monitored and their images used to help reduce accidents and traffic congestion. Another example occurs in the commercial domain for tracking factory installations and keeping the work flowing smoothly and efficiency.

B. WSN ARCHITECTURE

The specific characteristics of sensor nodes imply certain network implementations to deal with those issues. There are two types of network architecture: layered architecture and clustered architecture. They are described in the following section. [17,18,4]

1. Layered Architecture

As shown in Figure 1, the network is comprised of a Base Station (BS) and a number of layers, with each layer categorized with the same hop count. The BS gathers data from the closest nodes and broadcasts the fused data back to another base station or the user. The advantage of this technique is to allow short distance communications with low transmission power.

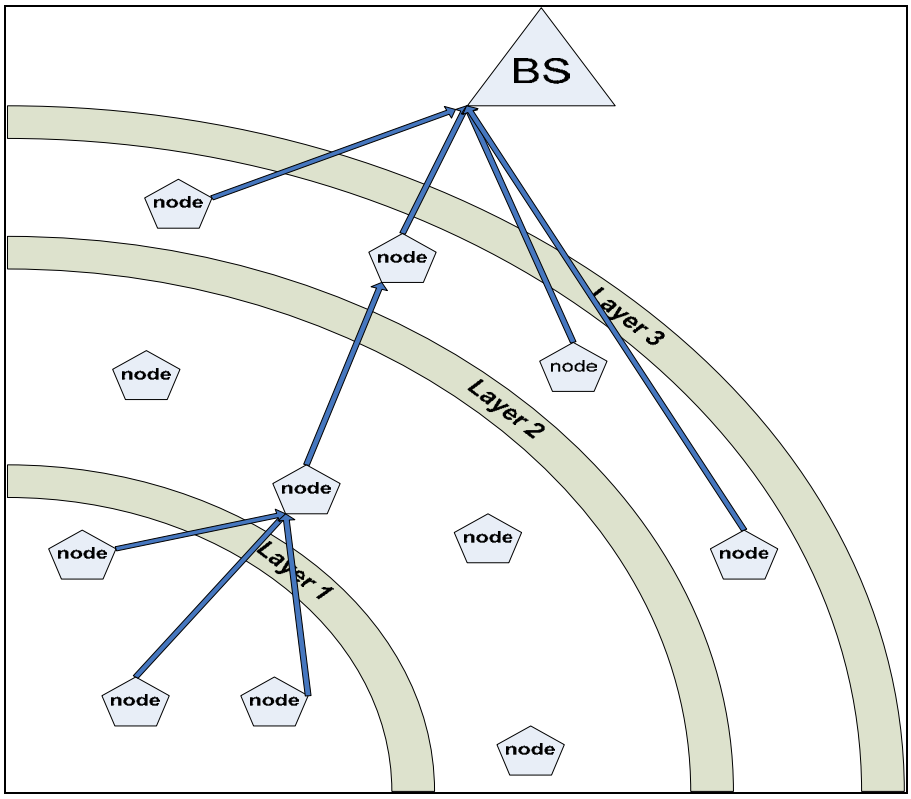

Figure 1. Layered Architecture (After: Ref. [19]).

2. Clustered Architecture

As seen in Figure 2, clustered architecture is another technique to group nodes in a specific area, comprised of a Cluster Head and Personal Area Network (PAN) Coordinator. Each Head and PAN Coordinator establish their own network of data collected, fused, and sent back to the base station (BS). Routing protocols, such as Low-Energy Adaptive Clustering Hierarchy (LEACH) are used to allow self organization.

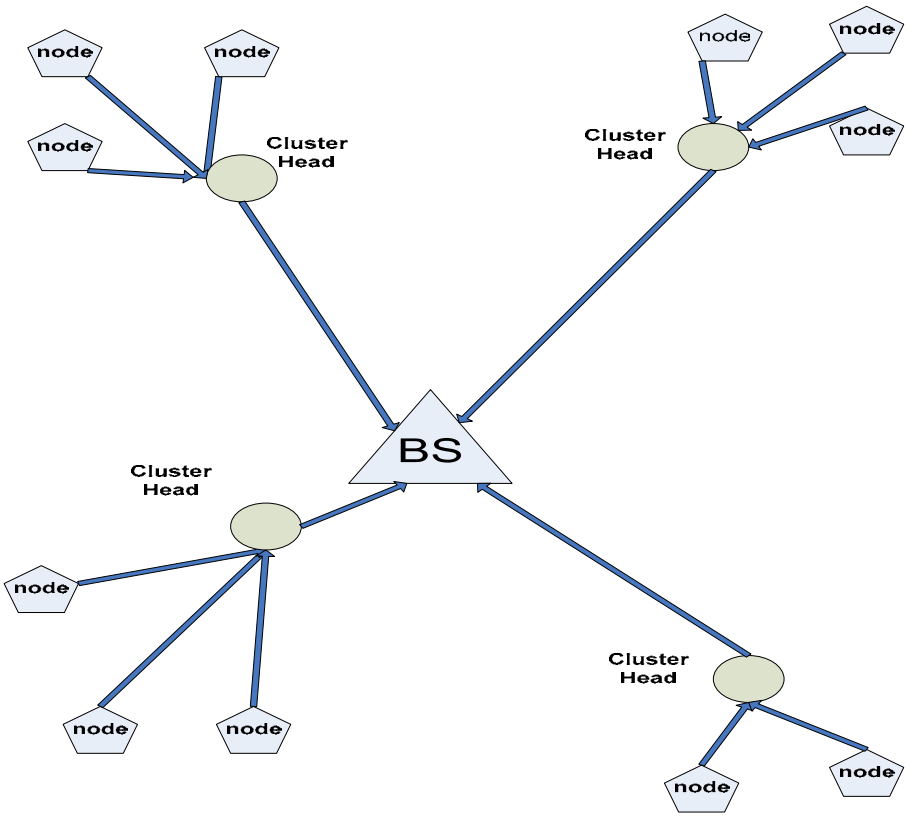

Figure 2. Clustered Architecture (After: Ref. [19]).

C. WSN STANDARDS

Standardization is a very important issue for the future of WSN technology, as it would make it cheaper and easier to integrate systems together since the devices are interoperable. There are widely accepted protocols such as the IEEE 802.15.4 Low Rate Wireless Personal Area Network (WPAN) standard (sponsored by the ZigBee Alliance Organization). These protocols are the focus of this thesis as they are used in MICAz motes.

1. The IEEE 802.15.4 Low-Rate WPAN Standard

This standard defines the protocols and devices rubric so that industry will implement the applications. The purpose of this standard is to specify the physical and MAC layer for the mobile device with less power dissipation, which usually operates within 10 meters. Also, in the design of these layers, cheap and simple implementations should be considered.

The data rate ranges between a maximum of 250 kbps and a minimum of 20 kbps. This standard should be flexible and tolerable for usage with different applications. The IEEE 802.15.4 standard works for star and peer-to-peer connections, which allows a variety of network topologies and routing techniques. In the standard, beacons may be used as they range at time intervals from 15.36 ms to four minutes.

The designer should compromise between power dissipation and message latency. To access the channel, CSMA/CA is used after a beacon. After that, contention access period (CAP) is sent. To assign logical addresses for devices, the address field is set to 16-bit long up to 64-bit. Acknowledgement is optional depending on the application. The standard allows nodes to go into a sleeping mode between beacons.

To use the ISM frequencies, the protocol should scan to find the most suitable channel. A Link Quality Indication (LQI) byte is added to each frame received and then sent to a MAC layer to provide information about the channel status, power control, location estimation, and routing protocol.

The nodes may operate in one of the following modes. The first is PAN Coordinator, which can initiate a network and is the primary controller of the network. The second is Coordinator, which can communicate with any device and the device in turn can only communicate with the PAN Coordinator or Coordinator. These roles categorize the nodes into two types: Full Function Device (FFD), which can work in any of the above roles, and Reduced Function Device (RFD) which is cheap, with minimal memory capability, and works in a “Device” role only.

The IEEE 802.15.4 standard comprises two physical layers: lower band, which operates at 868-868.6 MHz in Europe and 902-928 MHz in America and the Pacific rim, and the upper band, which operates at 2.400-2.485 GHz worldwide. Both lower band and upper band use Direct Sequence Spread Spectrum (DSSS). Table 1 depicts the specifications for the IEEE 802.15.4 physical layer.

PHY	frequency band		spreading parameters		data parameters		
	frequency	no. of channels	chip rate (kchips/sec)	modulation	bit rate (kbps)	symbol rate (kbaud)	modulation
868/915 MHz PHY	868-868.6 MHz	1	300	BPSK	20	20	BPSK
	902-928 MHz	10	600	BPSK	40	20	BPSK
2.4 GHz PHY	2.4-2.4835 GHz	16	2000	O-QPSK	250	62.5	16-ary Orthogonal

Table 1. Specifications for IEEE 802.15.4 Physical Layer (From: Ref. [20]).

2. The ZigBee Alliance

This alliance is a consortium created by most companies interested in this field of technology. Each company, based on their own requirements, adopted the IEEE 802.15.4 standard to make their devices interoperable.

The alliance contains more than 100 companies. Their goal is to build a low cost, low data rate, low power protocol to be used in wireless sensor network applications. They desire to standardize the upper layers, consisting of the industry representatives of all aspects, such as chip manufacturers, OEM manufacturers, service providers, and users.

The IEEE 80215.4 protocol stack consists of physical (PHY) and Medium Access Control (MAC) layers. The two layers are important due to the power limitation for the WSN. The physical layer operates at 2.4 GHz and 915 MHz. The channel access for the MAC layer is Carrier Sense Multiple Access/ Collision Avoidance (CSMA/CA). The ZigBee Alliance layers are network, security, and application. The network layer could be mesh, star, or a hybrid of both. The protocol stack is elaborated upon in Figure 3. The physical and MAC layers are defined in the IEEE 802.15.4 standard, and the ZigBee stack defines the upper layers.

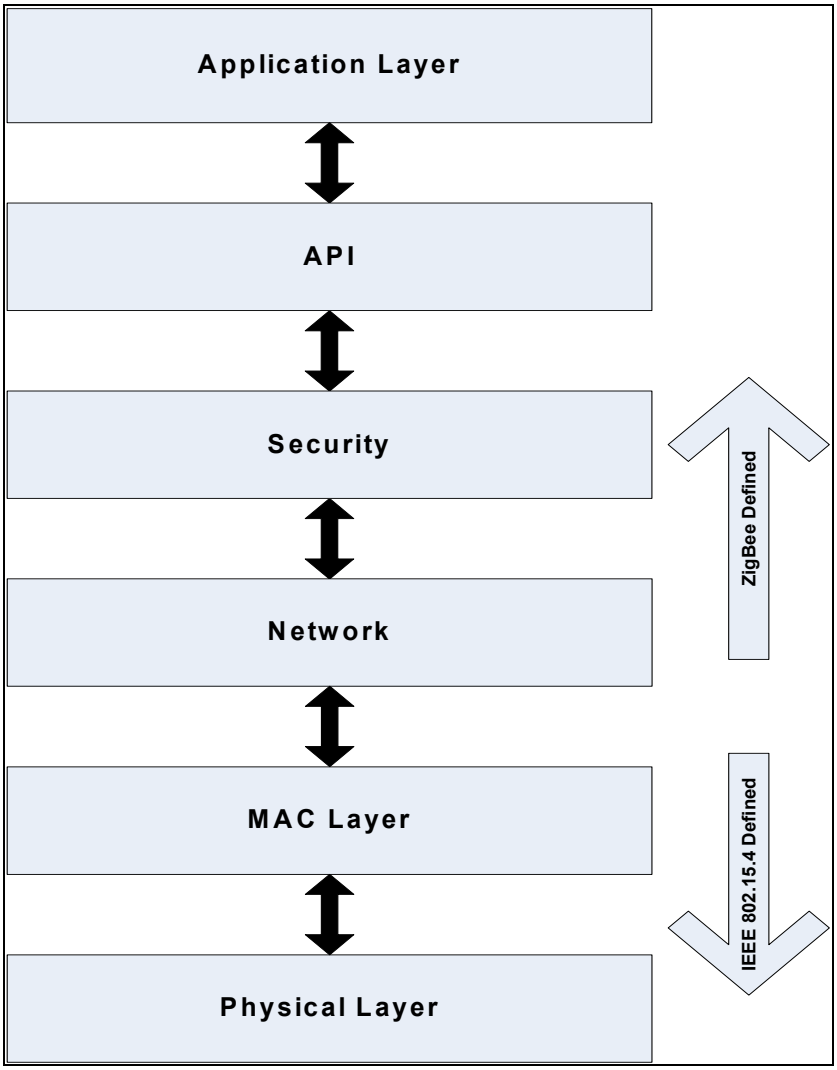

Figure 3. Protocol Stack for IEEE 802.15.4 and ZigBee Alliance.

3. Physical Layer

As shown in Figure 3, the general layered protocol stack of the WSN consists of the Application, Transport, Network, Data Link Layer, and Physical layers. The Physical layer is the most important for this thesis, and a brief discussion of this layer follows. [21]

The physical layer must perform many functions to activate and deactivate the transceiver, detect the channel power level, select the frequency of operation, and do the clear Channel Assessment (CCA) for CSMA/CA at the MAC layer. The Physical layer describes the communication of nodes, and the techniques proposed to be used for this layer are the PicoRadio, WINS, and the IEEE 802.15 family.

D. SUMMARY

This chapter provided a general overview of the WSN applications and other aspects and characteristics were discussed. Types of network architecture and wireless standards were introduced. In the next chapter, WSN antennas and propagation characteristics are discussed.

III. WSN ANTENNAS AND PROPAGATION

A. ANTENNAS

In the past, antennas were considered to be a secondary component for the sensor node. Recently, more attention is directed toward the design and implementation of the antennas. Antennas should cope with the small size of the node, which makes its implementation difficult. [22]

A physically small antenna design is possible when a high frequency is used. However, the difficulty arises when the frequency of operation is relatively low. In this case, electrically small antennas must be used. The following sections discuss some of the important aspects of WSN antenna specifications, design choices, RF performance, and the deviation from an isotropic pattern.

Directivity is generally not required for the WSN since the network is most likely to be deployed randomly. On the other hand, efficiency is an important design characteristic in WSN applications. To enhance efficiency, the impedance of the antenna and transmitter or receiver should be matched. The gain is directly proportional to the efficiency and the directivity characteristics of the antenna. As will be seen, when efficiency is low, the range will be less, so more power must be transmitted, or a more sensitive receiver must be used. [23]

Conducting and dielectric objects near the antenna could lower efficiency and influence the pattern thus causing deviation from isotropic. All antennas possess a property called the "keep out" region. Batteries, displays, sensors, and circuit boards should not be in this near-field region, which is calculated as $\lambda / 2\pi$ of the antenna [23]. At 2.4 GHz, this region is almost 2 cm in radius. The antenna designer should consider this problem in the case of the WSN. Some measures taken include placing the batteries and other metal objects as far as possible from the antenna.

In electrically small antennas, size, efficiency and the bandwidth are related to each other as follows [23]:

$$BW = \frac{2(2\pi d / \lambda)^3}{\eta} \tag{3.1}$$

where

BW = maximum instantaneous fractional bandwidth,

$2d$ = maximum dimension of the electrically small antenna,

λ = wavelength in meters, and

η = antenna efficiency which can be defined as $\frac{P_{radiated}}{P_{input}}$.

$P_{radiated}$ = power radiated by the antenna and

P_{input} = power into the antenna.

1. Antenna Design Choices and RF Performance

Every application poses a set of requirements on the design of the antenna. Internal antennas are preferable as they could be implemented cheaply and in small sizes. There are several common types [22]. First, the circuit board trace antenna is cheap, has thin dimensions, but by most measures it performs poorly. Second, the metal strip antenna performs better than the circuit board trace antenna and can be implemented as a dipole or loop. Third, a ceramic antenna component is simple in fabrication and installation, smaller than the metal antennas, but is more expensive. Finally, if the application for the WSN requires long range (relatively), an external antenna should be considered because it has high efficiency and better performance, at the expense of larger size.

Also, two other issues face the design of the WSN nodes: Electromagnetic Compatibility (EMC) and Electrostatic Discharge (ESD). EMC is an important feature as the nodes should work at the same location with other circuits and systems and their power may interfere with other systems operating in the same frequency band. Harmonics and the signal waveform are other players in the EMC problem.

The ESD problem is harder to identify and resolve, as it depends on several factors that pose a problem, mostly because of high density on integrated circuits that is driven by the need to keep costs low. Insulation and shielding can be used but it cannot completely stop this problem. Software and firmware programming could be used to lessen the probability and damage to the system.

B. RADIO PROPAGATION

The channel between the transmitter and receiver could be as simple as line of sight (LOS), but more likely the presence of objects such as buildings, mountains, and trees will create obstruction and provide multiple paths (multipath) for the waves to reach the receiver. Many models can be used to estimate the received signal, which are based on statistical or empirical data.

Multipath and fading are major players in the way channels affect the transmitted signal as it propagates through the media to the receiver. The electromagnetic wave propagation for wireless radio systems depends on three phenomena: reflection, diffraction, and scattering [23].

Reflection happens when the signal encounter a flat object with size much larger than the wavelength of the signal. Diffraction happens when the signal encounters a discontinuity, such as an object with an irregular surface and sharp edges. Scattering occurs when the signal encounters an object much smaller than the wavelength of the signal, such as rain drops.

Much research and many studies assume a simple model for radio propagation coverage, such as the free space model which neglects the earth. While more realistic models exist, such as the two-ray ground reflection model, it is still not precise enough for a complex environment such as inside a building.

The free space propagation model is used in the case of LOS between the transmitter and receiver. This model expects distance to be the major factor to determine the received power as stated in the Friis free space equation: [23]

$$P_r(d) = \frac{P_t G_t G_r \lambda^2}{(4\pi)^2 d^2 L} \tag{3.2}$$

where

P_t = transmitted power,

$P_r(d)$ = received power as a function of distance,

G_t = transmitter antenna gain,

G_r = receiver antenna gain,

d = distance in meters, and

L = system loss factor not related to propagation.

Equation (3.2) means that the signal is decaying proportional to the square of distance between the transmitter and receiver. The Effective Isotropic Radiated Power (EIRP) is defined as

$$EIRP = P_t G_t . \tag{3.3}$$

When unity gain and loss factor are assumed, the Path Loss (PL) determines the received power. In dB:

$$PL(\text{dB}) = 10\log\frac{P_t}{P_r} = -10\log[\frac{\lambda^2}{(4\pi)^2 d^2}] \tag{3.4}$$

Coverage and connectivity are important performance characteristics regarding the WSN. Coverage defines the way the sensor collects data in a specific region for a certain phenomenon. The distance could measure the level of confidence in this monitoring that the sensor's data could be collected with high credibility. [3]

Once the system parameters are defined, Equation (3.2) can be solved for R, which gives the sensor's range. The $\frac{1}{R^2}$ dependence is not seen in a complex urban or indoor environment because of multipath. The actual signal consists of small-scale fading

over tens of wavelength along with large-scale path loss. The large scale path loss may deviate significantly from $\frac{1}{R^2}$ but can often be approximated closely by some other path loss exponent, *n* as:

$$PL(\text{dB}) = -10\log[\frac{\lambda^2}{(4\pi)^2 d^n}] \tag{3.5}$$

Connectivity is simply how the network is connected together. Connectivity and Coverage cross in many ways as they affect each other. Most likely, when the connectivity is good, the network coverage is expanded. From the designer's prospective, they could be treated together [13].

C. RADIO IRREGULARITY

The ideal transmission model for a wireless sensor node with an omni-directional antenna is symmetric in all directions. Thus, the radio range and packet loss are constant and uniform in circular radius around the node as shown in Figure 4. In practice, this assumption is not true, as some researchers have shown this empirically for certain platforms. [1,3]

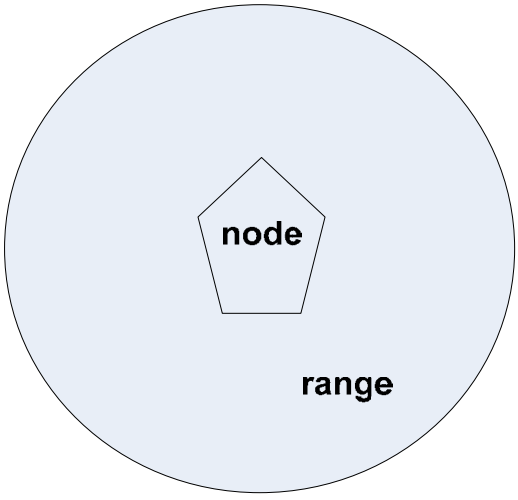

Figure 4. Regular Range around the Node (Ideal Case).

Radio irregularity is a significant factor in wireless sensor networks and cannot be ignored. It should be taken into consideration, since the propagation model will affect the

design and implementation of the network as well as the placement and topology of the nodes, especially in dense deployment cases. An example of irregular range for a node is shown in Figure 5.

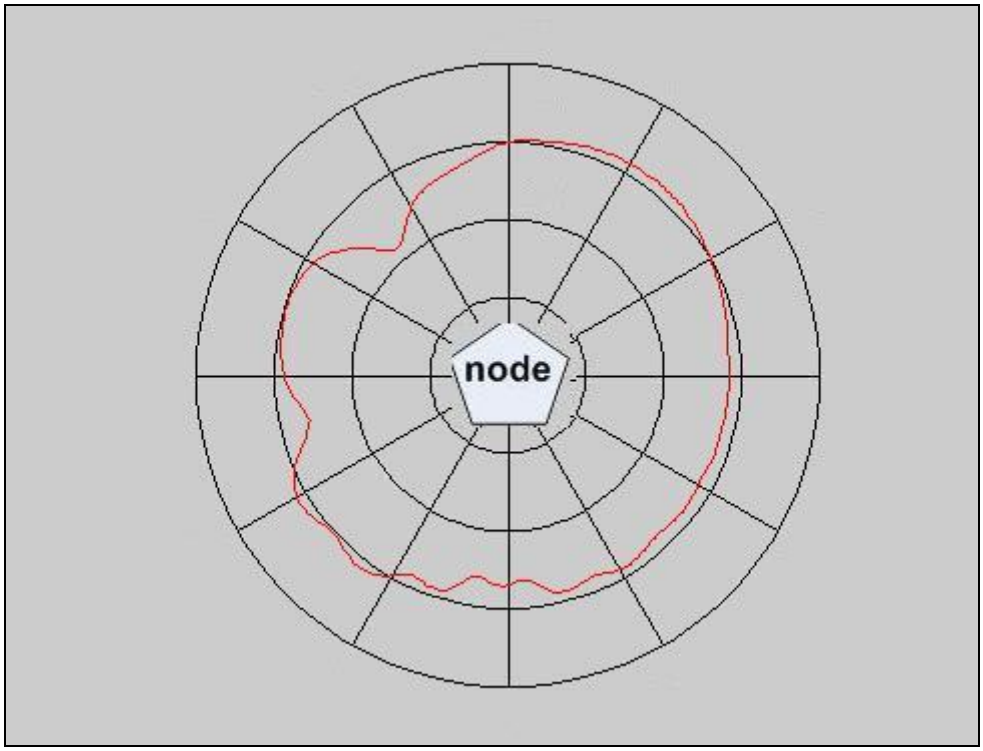

Figure 5. Example of an Irregular Range around the Node (Non-Ideal Case).

It is hard to conduct any experiment without an error margin due to different factors affecting the experimental setup. Often conducting an experiment with high accuracy is expensive and time-consuming, especially due to the large number of items included in the experiment. Simulation is the answer in this case. It will be cheaper and easier to use a simulation to obtain results when conducting an experiment than performing live experiments.

Radio irregularity affects the performance of the wireless sensor network protocols. Radio irregularity can affect MAC and networking protocols, and degrade their performance and ability to maintain connection to other nodes in the network.

Most protocols assume symmetrical radio transmission, so when this is not the case, the performance will not be as expected. Coverage protocols also have the same

assumption, and as that assumption is not true, coverage would be irregular, thus, leaving some areas without coverage. When two-dimensional flat earth models are considered, the terrain height and shadowing are neglected, which may not be accurate. [2]

Also, in addition to assumptions such as a flat earth and circular coverage other simplifications include: (1) all radios have the same output power, (2) the transmitter and receiver are reciprocal such that if one end receives a signal, the other end should also receive a signal when the transmitter and receiver are interchanged, and (3) range and signal power are simply proportional to distance squared.

D. MICAZ MOTES SPECIFICATIONS

Figure 6 elaborates on the common components of the sensor node in general. They are as follows: sensing unit, Analog Digital Converter (ADC), Central Processing unit (CPU), transceiver unit, and power unit.

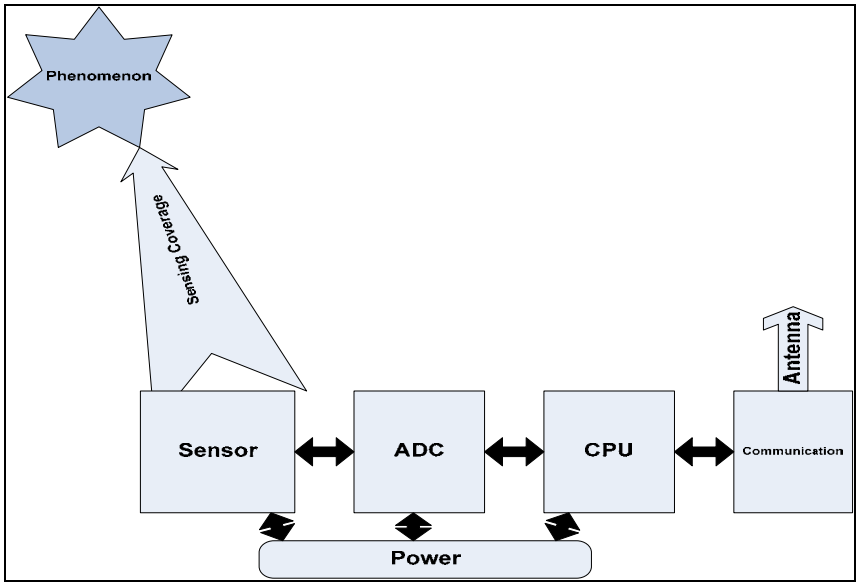

Figure 6. Components of Sensor Node.

The Crossbow Company produces several motes: MICA, MICA2, MICA2DOT, and MICAz. Figure 7 shows a picture of the MICAz mote, which uses a Chipcon CC2420 Processor/Radio Transceiver module and follows the IEEE 802.15.4 and ZigBee

Alliances at 2.4 GHz. The data rate is 250 kbps using a Direct Sequence Spread Spectrum (DSSS). [24] The coordinate system used for pattern measurements is also shown in Figure 7.

The processor runs an open source TinyOS operating system. The module comes with memory to store up to 100,000 measurements. Also, this module is capable of over-air reprogramming and possesses a battery power source with the possibility of an external power supply connection.

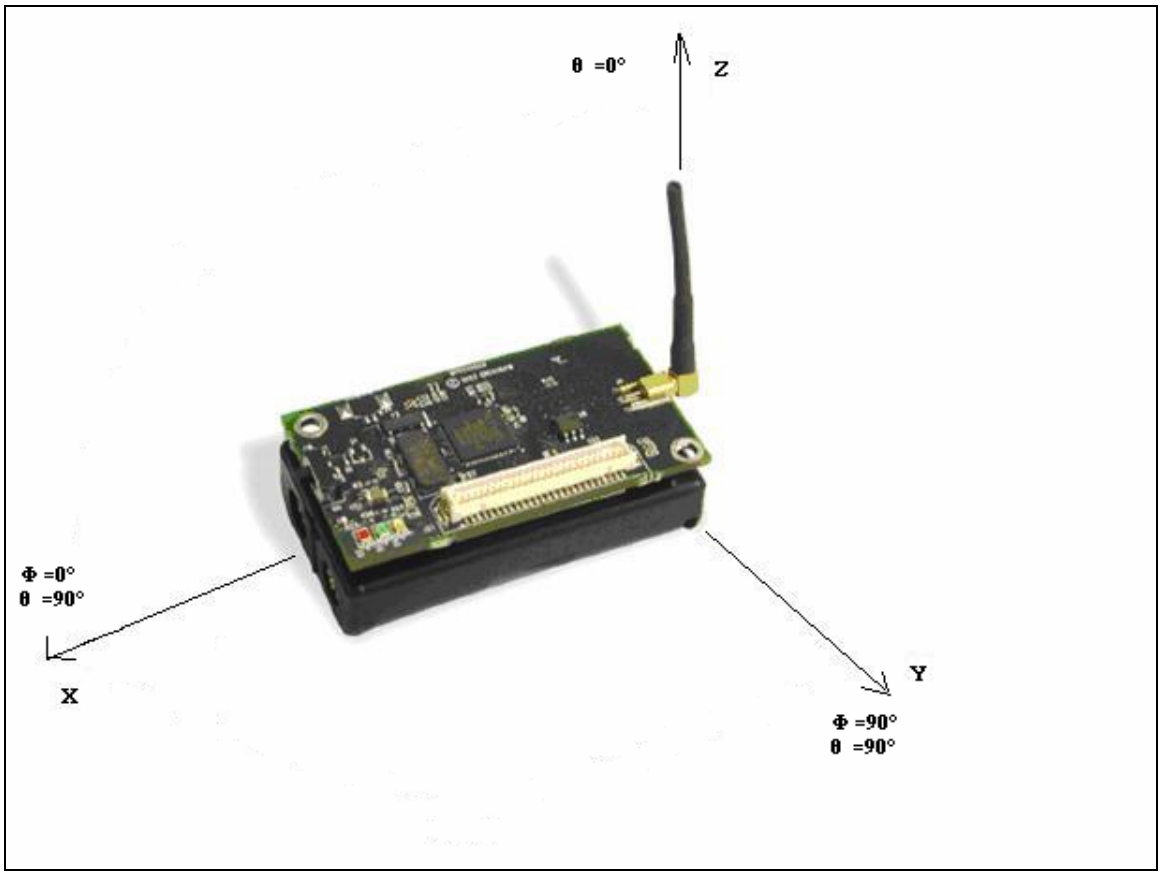

Figure 7. Photo of the MPR2400—MICAz with Standard Antenna (From: Ref. [24]).

The MICAz CC2400 radio is capable of tuning within the IEEE 802.15.4 channels, which start from 2.405 GHz to 2.480 GHz with a 5 MHz separation. The 2.405 GHz channel is selected by default.

RF transmission power can be programmed from 0 dBm to -25 dBm. It is preferable to choose the lowest transmission power, as it will reduce the interference and power consumption. Low power transmission keeps the range small, which reduces the probability of interference between motes. The RF Received Signal Strength Indication (RSSI) could be read directly from the CC2420 radio.

The regular antenna used with the MICAz mote is a $\frac{\lambda}{4}$ long insulated wire, which is called a monopole antenna. The length of the antenna operating at 2.4 GHz is 1.2 inches.

E. SUMMARY

This chapter discussed the propagation models for the WSN. The simplest of these models is the free space model. RF characteristics of MICAz sensor motes were presented as well**.** The architecture of the WSN and its components emphasizing the MICAz motes were also examined. In the next chapter, the experimental setup and simulation is introduced for different environments.

THIS PAGE INTENTIONALLY LEFT BLANK

IV. EXPERIMENTAL SETUP AND SIMULATION

Empirical data gathered using measurements in a real world environment and in a controlled environment such as an Anechoic Chamber will be compared with simulations created by software suites such as CST Microwave Studio, Urbana, and Rhino. This chapter presents the techniques and assumptions for these measurements and simulations.

A. MICAZ ANTENNA PATTERN MEASUREMENTS IN FREE SPACE

A radiation pattern is an important factor in antenna design. Some antenna parameters such as gain, half-power bandwidth, and side lobe level were determined by both simulation and measurement of the radiation pattern of the MICAz mote.

An absorber lined room is used to maximize the measurement precision. In this thesis, the measurements occurred in the Anechoic Chamber at the Naval Postgraduate School (NPS). The chamber is located in Spanagel Hall, Room 604.

To reduce reflections, the absorbers are mounted on the floor, ceiling, and the walls. These absorbers reduce reflection and attenuate fields, which will reduce multipath. The chamber design should duplicate the outdoor free space propagation environment. The Anechoic Chamber is described fully in [25]. Figure 8 shows the general structure of the NPS Anechoic Chamber.

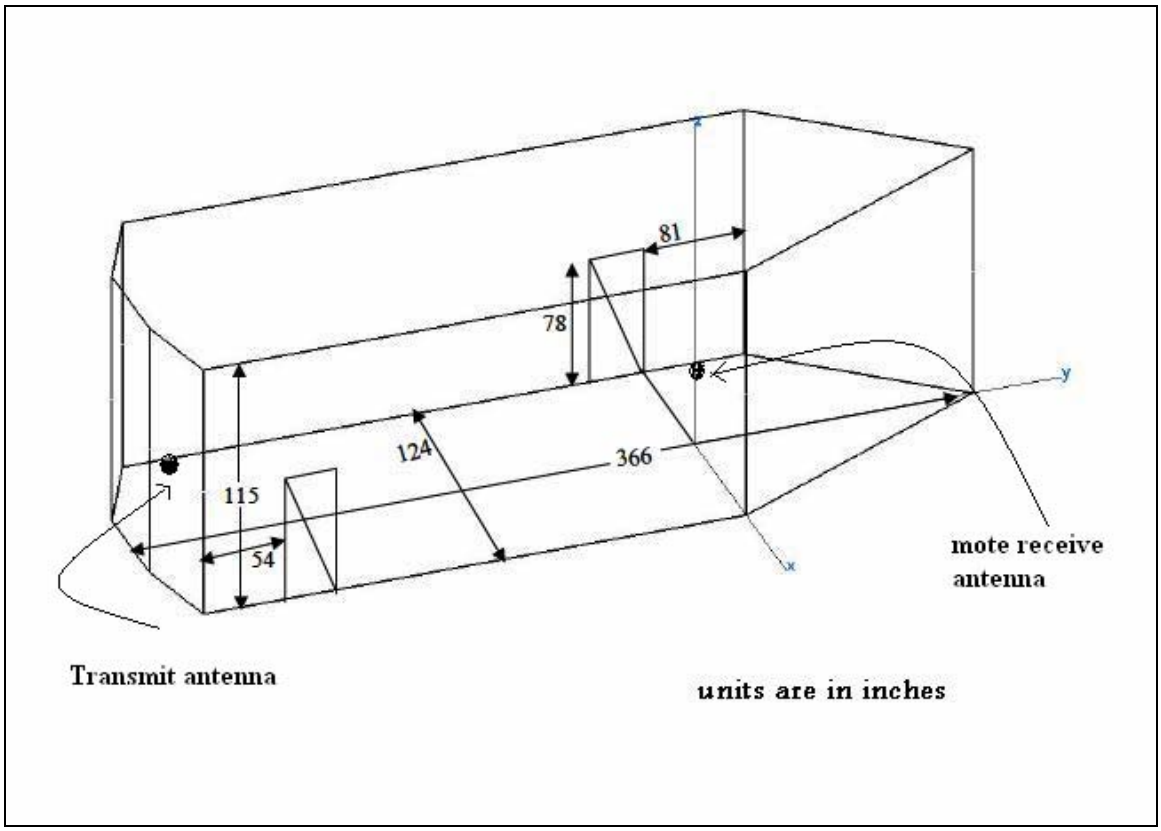

Figure 8. View of NPS Anechoic Chamber (From: Ref. [25]).

Figure 9 depicts the block diagram of the Anechoic Chamber antenna measurement system. The chamber is equipped with HP 8510, HP 8511, a coupler, and amplifiers. The equipment measures the transmitted power from transmitter to receiver and compares it to the power from a standard gain antenna. The distance between the transmitter and receiver is equal to 5.8 meters.

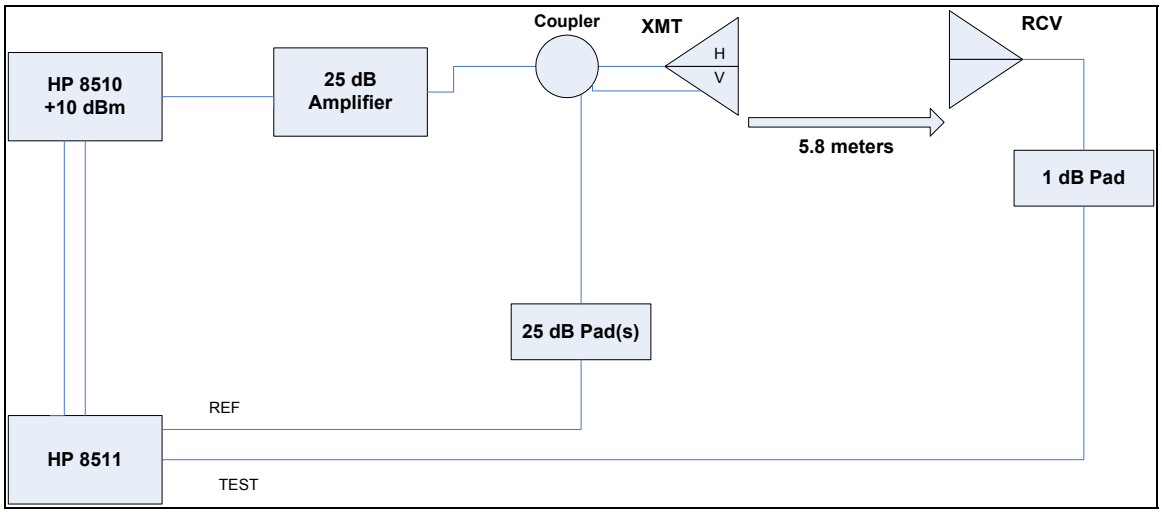

Figure 9. Block Diagram of NPS Anechoic Chamber.

The antenna radiation pattern and gain are important aspects of the MICAz motes discussed in this section. In the first measurement, the free space radiation pattern of the mote is to be determined.

A prototype of the MICAz was built to mount the mote's monopole antenna. An adaptor is used to connect the antenna to the measurement platform. The Automated Antenna Pattern Measurement Software installed in the chamber's equipment performs the measurements automatically and the results are gathered into an output file for analysis.

A horn antenna is used at the transmitter side with 2.48 GHz frequency. The MICAz mote prototype is on the receiving side, which is rotated by the system automatically during the measurement to obtain a 360˚ pattern. The measurements are repeated for the horizontal orientation of the transmitting and receiving antennas. Figure 10 shows a picture of the Anechoic Chamber and its control equipment. Figure 10.a depicts the interior of the chamber showing the transmitting and receiving pads. Figure 10.b shows the control equipment which consists of the HP rack and the computer which has the software to process and manage the system functions.

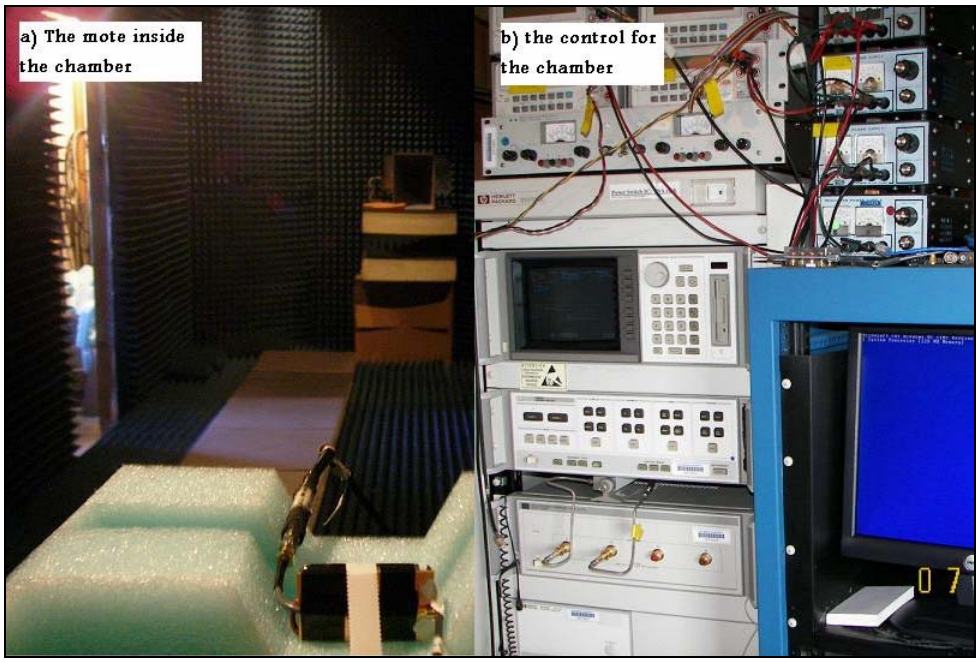

Figure 10. a) The MICAz Prototype in the Anechoic Chamber. b) The Control Panel for the Chamber.

The MICAz model is raised one meter above the floor, which is absorber lined to minimize the ground plane interference. In this study, the ground plane effect is ignored. Also, only the principal polarization was measured; no cross-polarized patterns were measured. The mount only rotates in azimuth (the horizontal plane).

Figure 11 shows the software installed on the computer in the Anechoic Chamber. It shows the gauges and controls for different components of the experimental setup. It also shows the position of the receiving system rotating 360˚.

The antennas were deployed in four positions as seen in Figure 12. First, is a horizontal cut (*x*-*y* plane); second, is a vertical cut (*y*-*z* plane); third, it is vertical cut (*x*-*z* plane with tilt to the right); and fourth, it is vertical cut (*x*-*z* plane with tilt to the left). The purpose of the tilt was to identify any chamber reflections in the pattern.

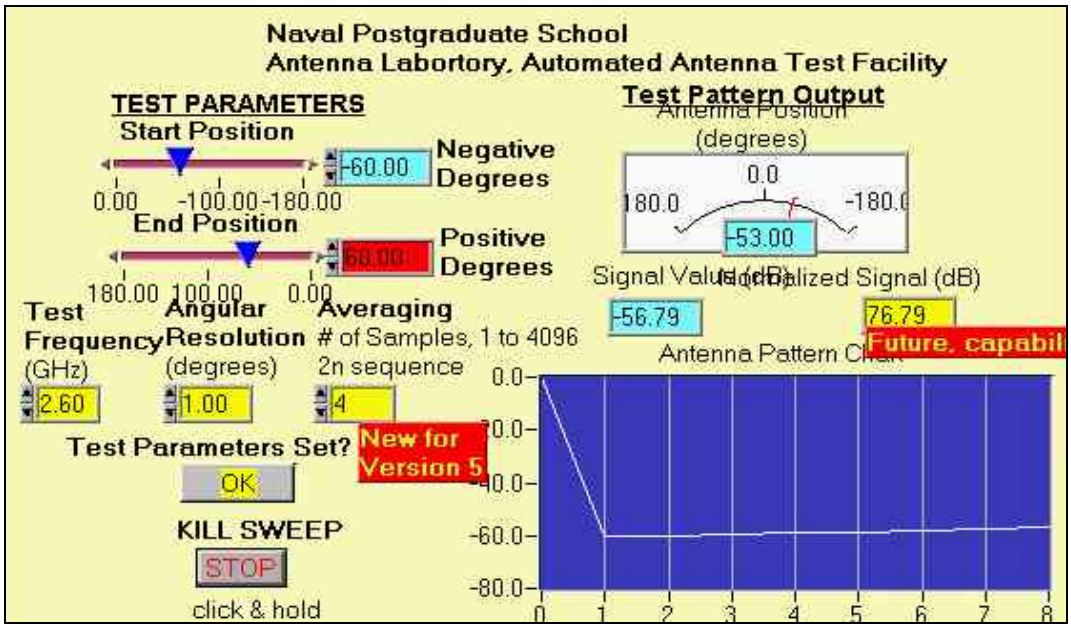

Figure 11. Screen Shot of the Software which Controls the Anechoic Chamber Measurements.

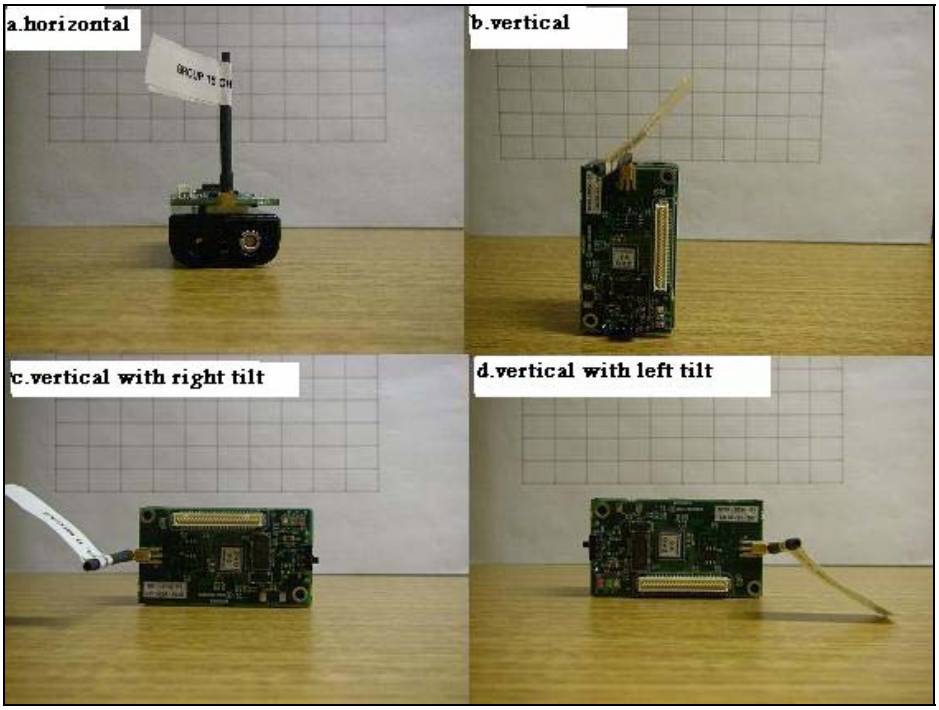

Figure 12. Multiple Test Position for the MICAz Mote, (a) Horizontal Cut Plane, (b) Vertical Cut Plane, (c) Vertical Cut Plane with Right Tilt, and (d) Vertical Cut Plane with Left Tilt.

The output file for the first position measurements was processed using MATLAB software. Figure 13 shows the diagram of the horizontal cut of the measurements. The radial units are the received power in dBm. It shows that the pattern is almost omni-directional for the monopole antenna. By substitution with a reference antenna, the gain was found to be approximately 0 dBi.

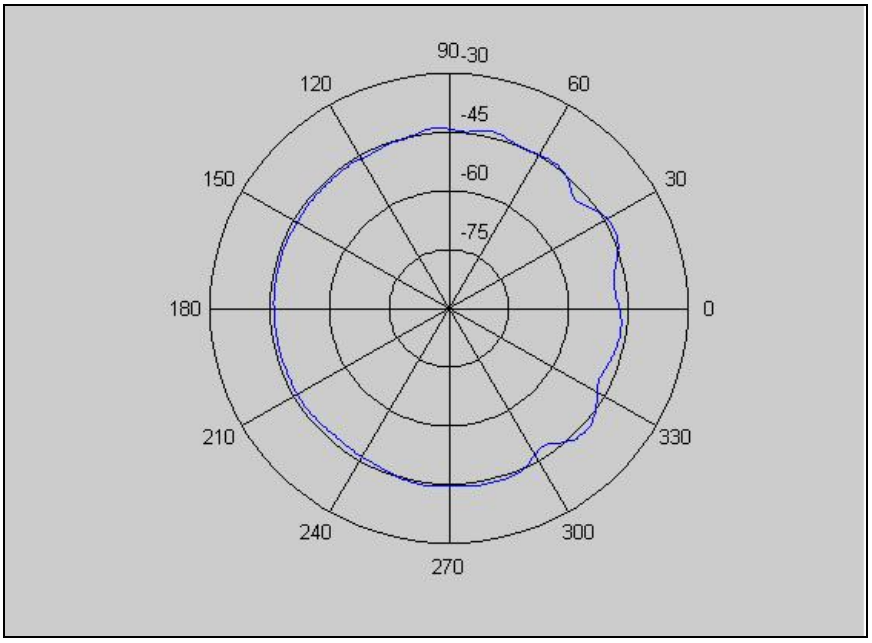

Figure 13. Pattern Shows the Horizontal Cut Plane of the Measurements.

The graph in Figure 13 shows that the MICAz radiation pattern is uniform to within a couple of dBm. The ripple on the right hand side is due to the metallic board of the mote and the edge location of the antenna contributes to the non-uniform behavior of the pattern.

In the second setup as shown in Figure 12.b, the vertical cut plane, is measured following the same technique used in the first part of the experiment. Figure 14 depicts the graph of these measurement results. The radiation pattern in this case is different as it shows the characteristic nulls (notches) of the monopole antenna.

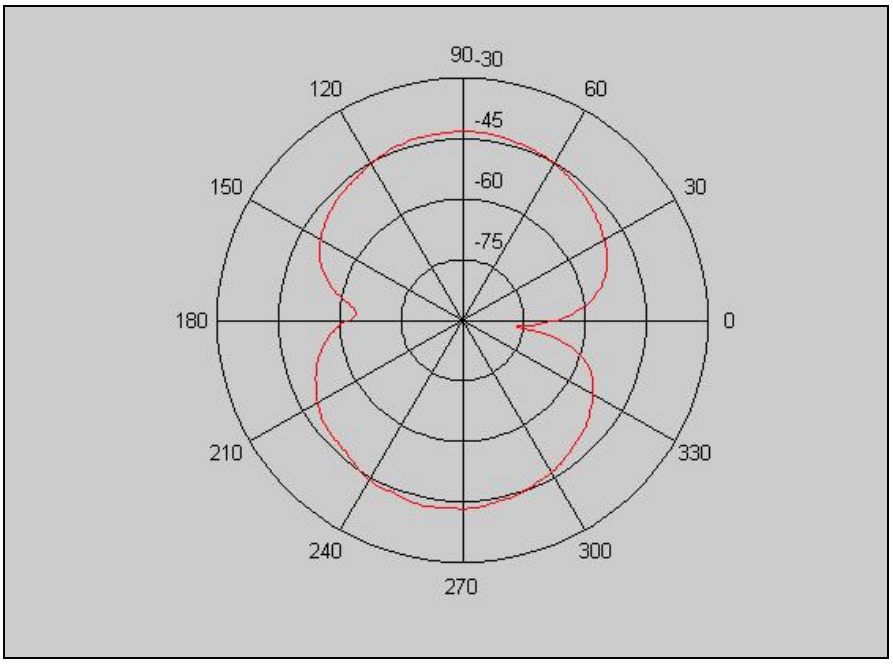

Figure 14. Pattern Shows the Vertical Cut Plane of the Measurements.

To explore the effects of chamber reflections on the vertical cut plane more in depth, the third and fourth experimental setups are conducted according to Figures 12.c and 12.d. These two experiments were done in different tilt directions. Measurement results are shown in Figures 15 and 16. These graphs show a similar radiation pattern with a 90˚ rotation. They show a more uniform pattern resulting from the reduced effect of the mote board.

The two experiments, which created Figures 15 and 16, resulted from two positions in the Anechoic Chamber. Ideally, the two patterns should be identical if rotated by the tilt angle. Any difference is due to reflections from the chamber walls, which change with tilt angle. The gain in cases 12.b, 12.c, and 12.d is slightly more than zero due to the effect of the mote board position with respect to the antenna.

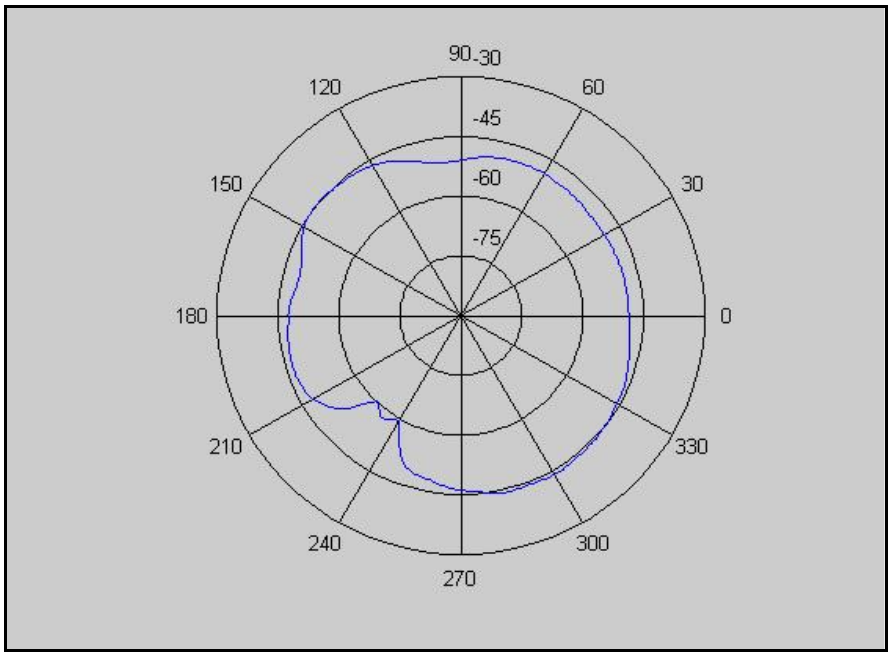

Figure 15. Pattern Shows the Vertical Cut Plane with Right Tilt of the Measurements.

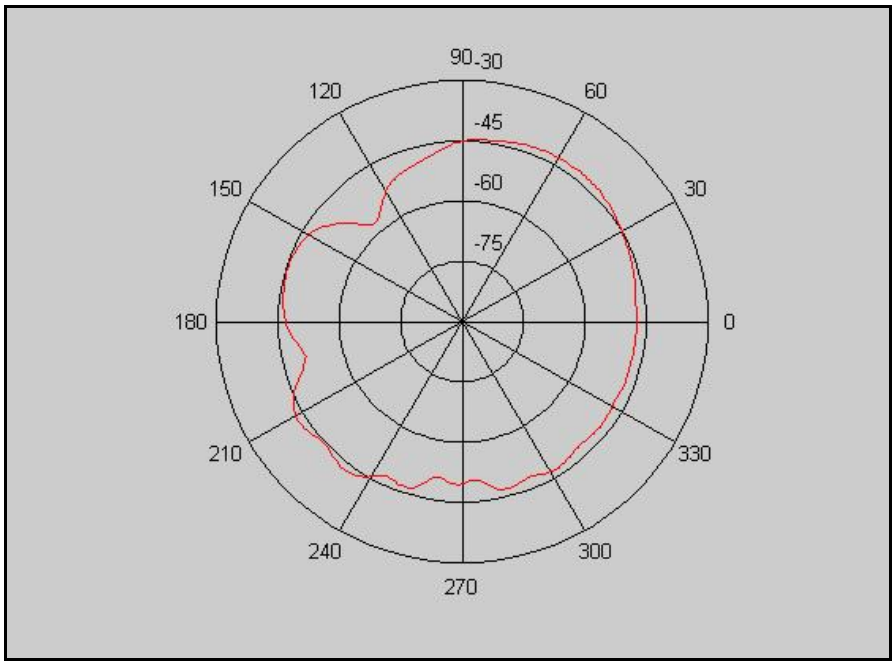

Figure 16. Pattern Shows the Vertical Cut Plane with Left Tilt of the Measurements.

B. SIMULATION FOR MICAZ MOTE ANTENNA

To simulate the MICAz mote in free space, a numerical electromagnetic code was used. Microwave Studio by Computer Simulation Technology (CST) is a tool for fast and accurate 3D EM simulation of high frequency problems. Along with a broad application range, the CST Microwave Studio offers a considerable product to market advantages such as shorter development cycles, virtual prototyping before physical trials, and optimization instead of experimentation. It uses the finite element method and therefore is capable of computing the effects of objects in the antenna's near field.

The MICAz mote model was built using this simulator to demonstrate its radiation pattern. Figure 17 depicts the models created in the CST Microwave Studio. Figure 17.a shows a simple model, while Figure 17.b shows a more detailed model created to provide more accurate results. The advanced model takes into account the dielectric material of the battery pack and the conducting material of the circuit board.

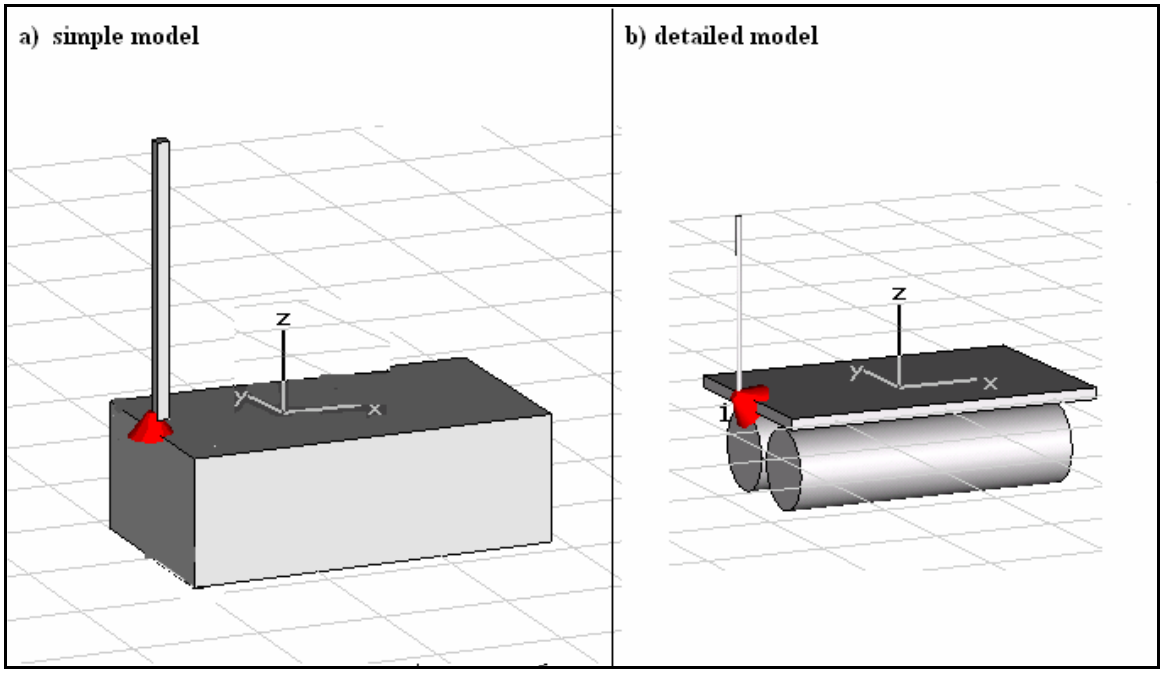

Figure 17. MICAz Mote Built in CST Microwave Studio. a) Simple Model. b) Detailed Model.

The dimensions of the model are the same as the actual dimensions of the mote, which are 56 mm on the *x*-axis, 18 mm on the *z*-axis, and 36 mm on the *y*-axis. The antenna length is 32 mm with 1 mm diameter. The CST Microwave Studio system calculates the expected radiation pattern for the model in three dimensions. Figure 18 shows the three-dimensional graph of the pattern for the mote in free space.

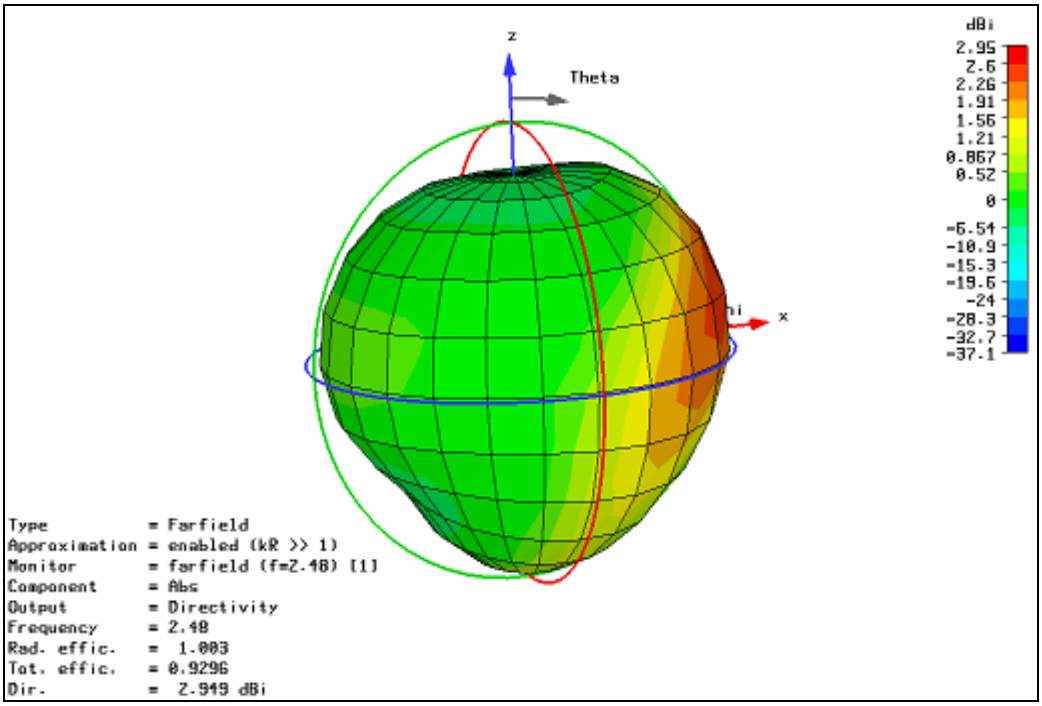

Figure 18. 3-D radiation Pattern for the MICAz Mote (Simple Model).

This specific output graph shows the directivity of the radiation pattern. If the gain is calculated for the window toward the *x*-axis, it will be 3.332 dBi as shown in the graph. For a better viewing of the results, the system created multiple cuts of the pattern at different angles.

Vertical and horizontal cuts were created and are shown in Figures 19 to 21. Figure 19 depicts the graph of the radiation pattern for horizontal cut plane calculations of the model. The graph is similar to the graph in Figure 12, which was created from real measurements in the Anechoic Chamber.

The differences between the measurements (Figures 14 to 16) and simulations are due in part to inaccuracies in the experimental setup in the Anechoic Chamber. The

simulation is for the simple model of the mote isolated in free space, where as the measurement is taken above a ground plane. Also, the box is assumed to be a perfect electric conductor in the CST model.

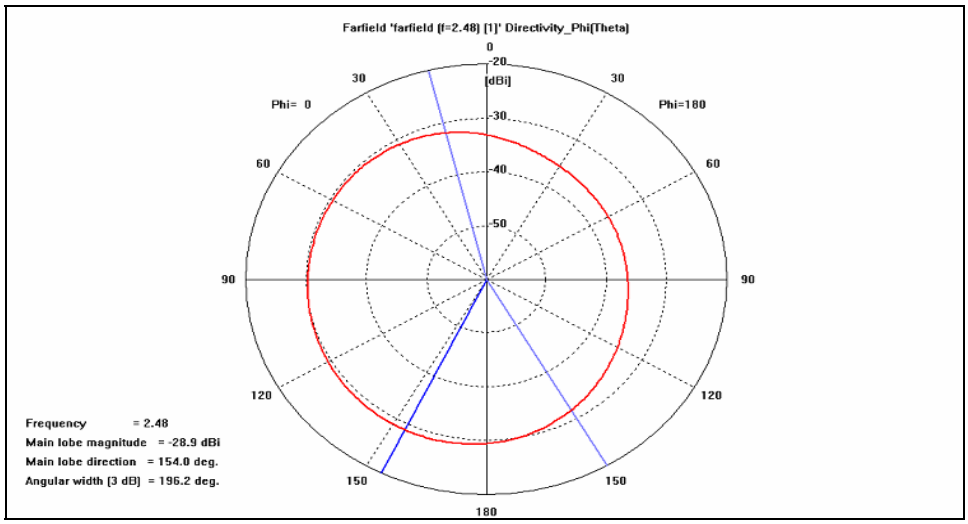

Figure 19. The Radiation Pattern for the Horizontal Plane (Simple Model).

Figure 20 depicts the graph of the radiation pattern for vertical cut plane calculations of the simple model. The graph is similar to the graph in Figure 14, which was measured in the Anechoic Chamber.

Again, minor differences in the null depths occur due to the experimental setup explained above. Also, the orientation of the graph has a 90˚ offset because of the different coordinate system reference between the experiment and simulator.

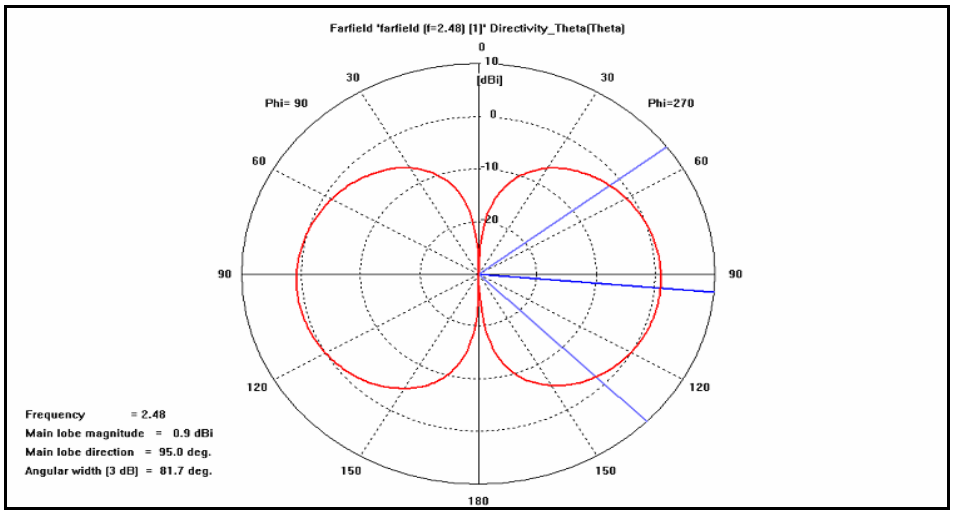

Figure 20. The Radiation Pattern for the Vertical Plane (Φ =90°) (Simple Model).

Figure 21 depicts the calculated graph of the radiation pattern for vertical cut of the simple model. The graph is different from the graphs in Figures 15 and 16, which were created from real measurements in the Anechoic Chamber.

Figures 15 and 16 resulted from the two rotated positions according to Figures 12.c and 12.d. If rotated appropriately, they should agree with the result in Figure 21. However, the nulls are deeper in the simulated pattern because of the free space environment and perfectly conducting material.

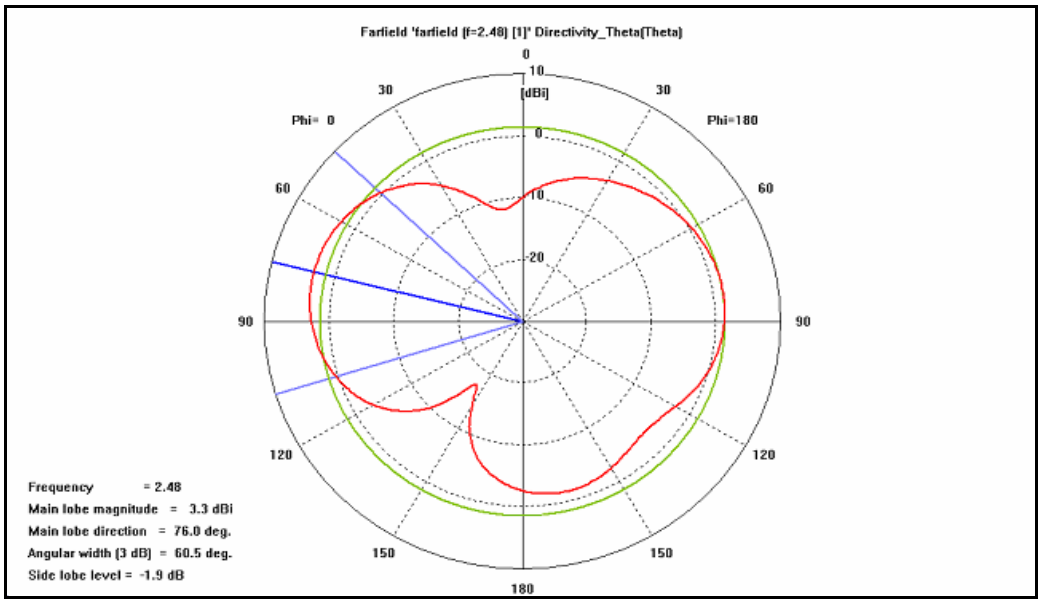

Figure 21. The Radiation Pattern for the Vertical Plane (Φ=0°) (Simple Model).

Comparing the results of experiment and simulation shows the asymmetry of the radiation pattern in the free space model. The fact that there are no external factors in the free space model implies that those irregularities are characteristic the mote antenna itself. The asymmetrical pattern is a well-known phenomenon that occurs when electrically small antennas are mounted on small objects.

The end user should plan the deployment with respect to the irregularity issue. In this study, the next experimental setup is to measure the radiation pattern in an environment with multipath and fading effects. Simulations are used to predict signal levels and the results are compared with measurements.

C. MICAZ ANTENNA PATTERN MEASUREMENTS IN THE FIELD

In Sections A and B, the radiation pattern for the MICAz mote was measured and simulated in free space. The next step was to measure the radiation pattern for the mote in the field. The location chosen for this experiment was the roof of Spanagel Hall. Figure 22 shows a picture of the location.

Figure 22. Picture of the Roof of the Spanagel Hall.

This specific location was selected for several reasons. First, as simulation is the next step, it was necessary to control the people and vehicles entering the location, which reduced the possibility of having reflection and multipath from sources that would have to be included in the simulation. The surfaces are flat and open, and are easy to simulate as opposed to objects such as trees and metal stairways. Lastly, the selected location is convenient and has the required power supplies and equipment.

The MICAz mote was used for this experiment to transmit power while the base station mode was connected to a laptop using a communication board. MOTE VIEW 1.0 is installed on the laptop. Another MICAz mote was also in use to ensure that both motes communicated with each other.

An Agilent E4405B ESA-E Series Spectrum analyzer was used, with a CUSHCRAFT S2406P antenna of 6 dBi gain from 2.4 GHz-2.50 GHz, was used to receive the signal so that it could be analyzed and processed. A Low Noise Amplifier (LNA) is necessary, as there is a lot of interference on the channel at this frequency, so a WJ-5004-116 LNA with 26 dB gain was be used, which operates from 2-4 GHz.

An H-1498 pyramidal horn antenna, by Antenna Electronic Laboratories (AEL), was attached to the spectrum analyzer as a receiving antenna. The specifications for this antenna are not available and thus, they were measured. The antenna gain measurements took place in the Anechoic Chamber, described earlier in this chapter. The AEL horn antenna operates from 2-18 GHz. Figure 23 shows the antenna in the Anechoic Chamber.

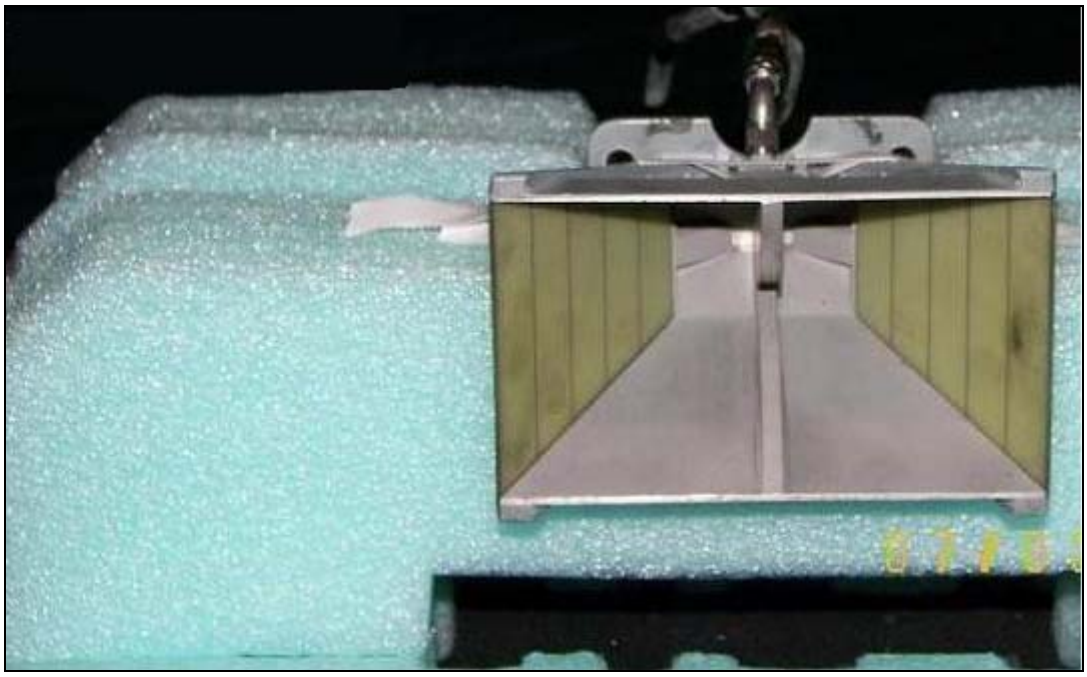

Figure 23. The AEL Pyramidal Horn Antenna at the Anechoic Chamber Gain Measurement.

The resulting file is processed by the MatLab software to obtain the gain, directivity and other characteristics of the AEL horn antenna. Figure 24 depicts a graph of said data.

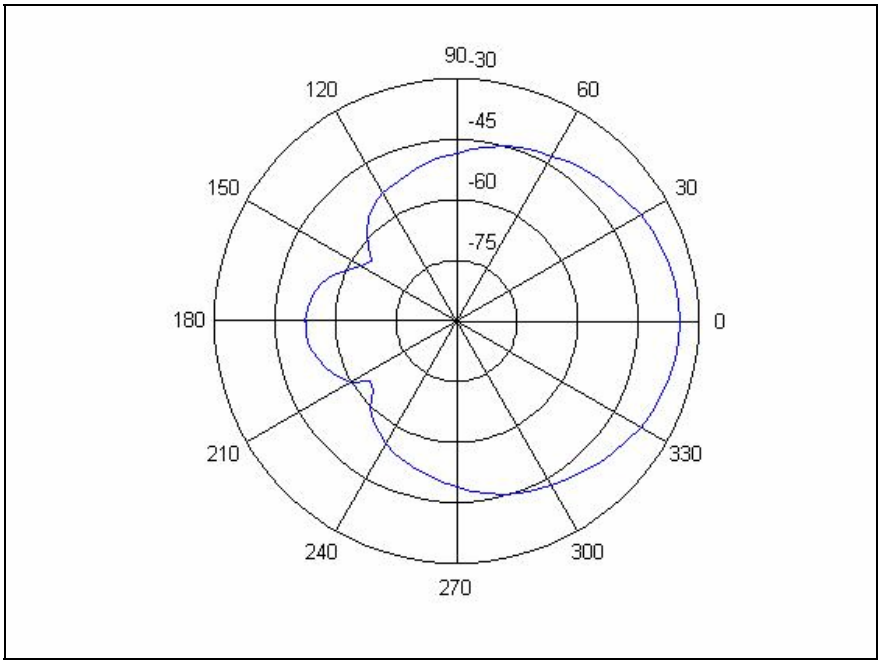

Figure 24. Picture of Radiation Pattern for the AEL Pyramidal Horn Antenna.

The graph shows the directivity and gain for this antenna. The gain at 2.48 GHz frequency is measured to be 8.54 dB. The resulting measurements for the AEL horn antenna at different frequencies will be fed to the Agilent E4405B ESA-E Series Spectrum Analyzer so that it will be included in its measurements (i.e. it will be taken out in the normalization). The experimental setup is shown in Figure 25. The MICAz output power was measured earlier using the Agilent measurement system to be -35.82 dB. The received power is calculated from:

$$P_r\,(\text{dB}) = -35.82\ \text{dB} - \text{Path Loss dB} - 8.54\ \text{dB}. \qquad (4.1)$$

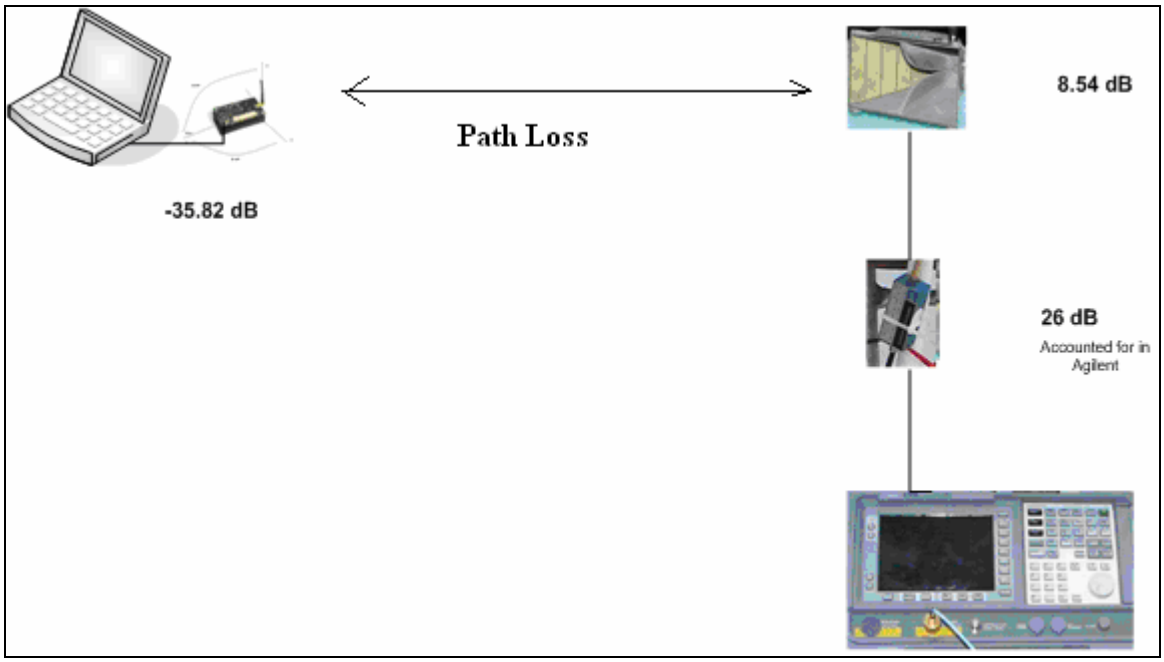

Figure 25. Diagram of the Experimental Setup

1. First Configuration

The first measurement set had a MICAz mote at the position specified in Figure 26. The power measurement system, which is the Agilent E4405B ESA-E Series Spectrum Analyzer System, was moved to multiple locations on the roof as seen in Figure 26.

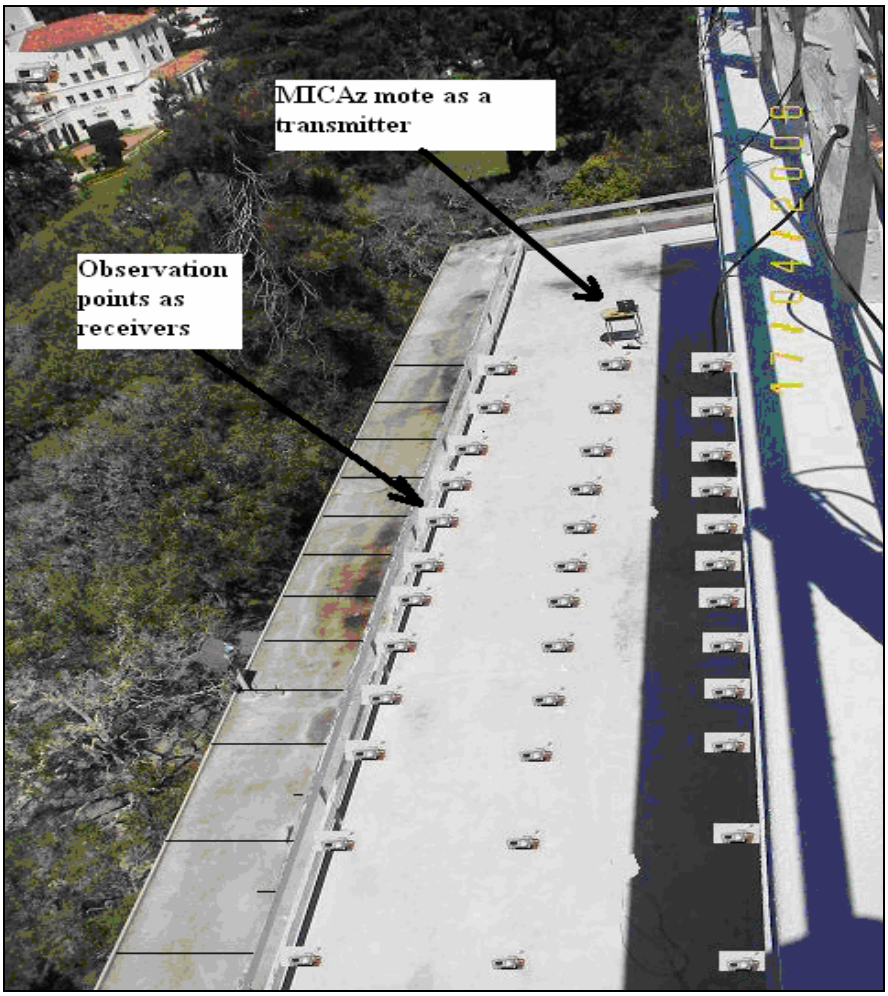

Figure 26. Locations of the Power Measurement System on the Roof of Spanagel Hall.

Three measurements are taken at each location so that an average of three measurements is considered to be an accurate value at that specific location. The locations of the receiver look like an equally spaced mesh while the nodes of the mesh are the locations of the receiver.

Figure 27 shows a contour plot of the resulting data. The received power level in dBm measured at each location. Power levels are color coded to make to make the pattern of the signal distribution clearer for the reader. Power levels from -100 dBm to -90 dBm are represented as dark blue. Power levels from -90 dBm and -80 dBm are represented as red. Power levels from -80 dBm and -70 dBm are represented as white. Power levels from -70 dBm and -60 dBm are represented as light blue.

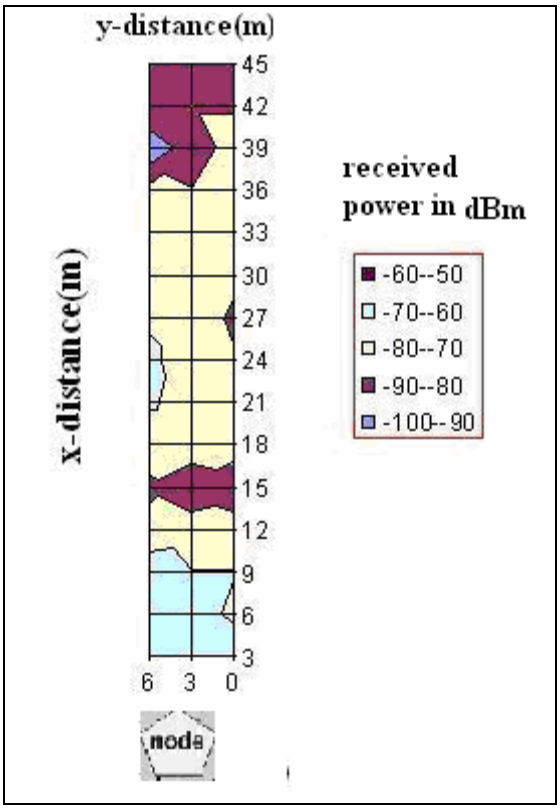

Figure 27. The Distribution of Received Power around the MICAz Mote.

According to Equation (3.2), which is the Friis equation, the power distribution is inversely proportional to distance squared, which means that power gets lower with respect to the distance squared between the transmitter and receiver. As seen in Figure 27, the effect of multipath is obvious, as the power distribution around the transmitter is decreasing gradually according to the Friis equation.

In this environment of multipath and fading, the received power is sometimes lower at points closer to the transmitter than when the distance is far away. This fluctuation is due to the adding and subtracting of the transmitted signals from direct path and multipath, as well as diffraction from edges and corners.

As the operating frequency of 2.48 GHz is in the ISM band, another factor that contributes to the signal fluctuations is due to the interference of signals from other

anonymous transmitters around the experimental location. The exponent value *n* in Equation (3.5) is calculated for this environment to be 2.4, which implies an environment close to the free space exponent.

2. Second Configuration

The next experimental setup adds another factor to the measurement, which is the human presence. For the test a human will be located between the transmitter mote and the receiving system as seen in Figure 28.

Figure 28. The Experimental Setup for Human Presence between Transmitter and Receiver.

First, the received power is measured when the human is not present. The value is equal to -70.3 dBm as marked in Figure 29 with a red line. Next, the received power is measured while the human stands at different locations between the transmitter MICAz mote and the receiver. The transmitter and receiver location stay fixed. Figure 29 shows the effect of human presence in terms of the power received in dBm.

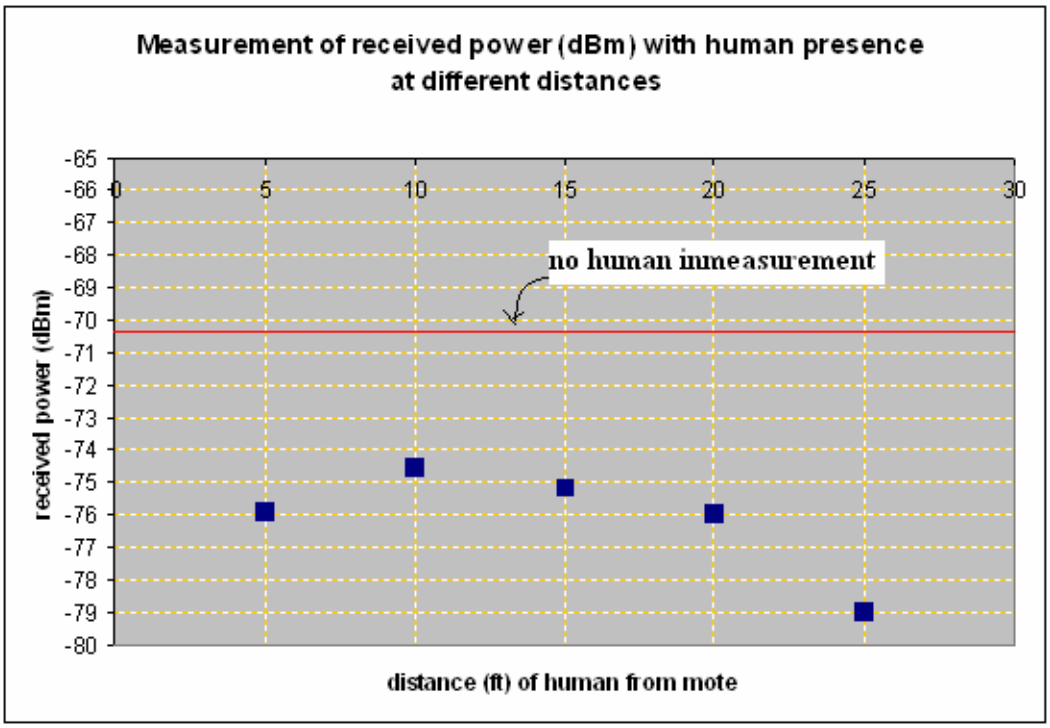

Figure 29. Measurement of the Received Power (dBm) with Human Presence at Different Distances.

As seen in Figure 29, for measurements with the experimental setup, the effect of the human presence is greatest when the human is close to one of the antennas.

3. Third Configuration

The next stage of the measurements should be examining the effect of the deployment of multiple MICAz motes. These motes should transmit in sequence and the measurements should take place for each mote to build the overall picture of the radiation pattern of these motes together.

This stage could not be implemented due to several reasons. The first problem was that there is no suitable measuring equipment capable of collecting the signal from each mote and storing those values for that specific mote when they are all transmitting.

The other problem is that the mote's trigger for transmission was not controllable due to the proprietary software responsible for that. The other issue related to this experimental setup is that an approximation could be used in the case of multiple motes. The reason behind that approximation is that these motes usually will not transmit all at the same time.

The master mote will send a packet and the slave mote will receive and process these packets. After that, the slave motes will start transmitting in turn. This mechanism will make the effect from one mote to another negligible. The multipath and fading factor are in effect at certain distances and environments.

Therefore, with the equipment available, it is not possible to isolate the multipath effect and study its relationship regarding the irregularity of the propagation pattern in the multiple motes environment. Future work will be needed in this area of research.

D. SIMULATION FOR MICAZ MOTE IN THE FIELD

To simulate the environment in which the field measurements were taken, it was necessary to create a similar structure in the software. The Urbana simulator, by Science Application International Corporation (SAIC), was used to simulate the environment around the mote.

The Urbana 3-D Wireless Toolkit computes radio signal propagation in different complicated environments. Urbana is comprised of two major components: iUrbana and Urbana_comp. iUrbana is a GUI front-end which provides simulation settings, 3-D visualization, and user scenario configuration to display simulation results. Figure 30 depicts the iUrbana main window.

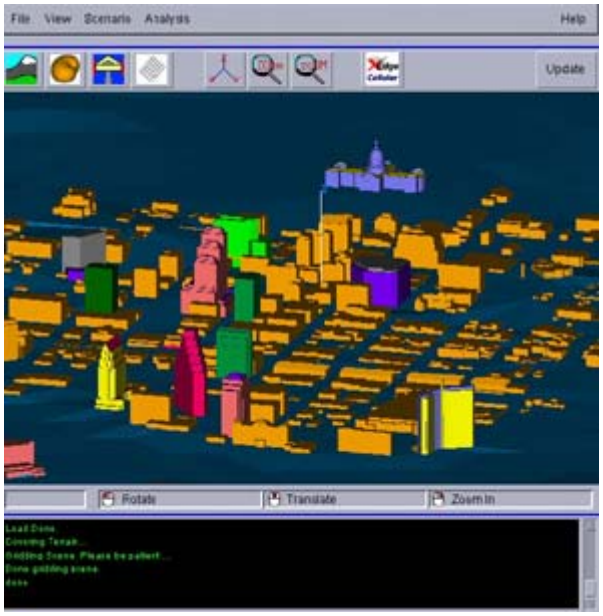

Figure 30. Picture of iUrbana Main Window.

Urbana_comp is a standalone back-end application which processes the simulation code. It also can process batch jobs without user intervention. Urbana_comp controls two other applications: Urbana and urbana_rp which are transparent to the user and run analysis calculations for data provided by Urbana_comp. [20]

The simulation process occurred in steps starting with the creation of the location of the experiment and the mote model, and then feeding those models into the Urbana simulator. These processes included many file conversions and manipulations to make the required simulation environment work coherently.

The location of the experiment as mentioned previously was the roof of Spanagel Hall at NPS. After measuring the dimensions of the building, the model for the building was created in the Computer Aided Design (CAD) tool Rhinoceros (Rhino). The Rhino simulation tool by Robert McNeel & Associates is a sophisticated simulation tool similar to AUTOCAD software which specializes in building models for objects such as buildings, trees, cars, and so forth. Figure 31 depicts the Rhino screen.

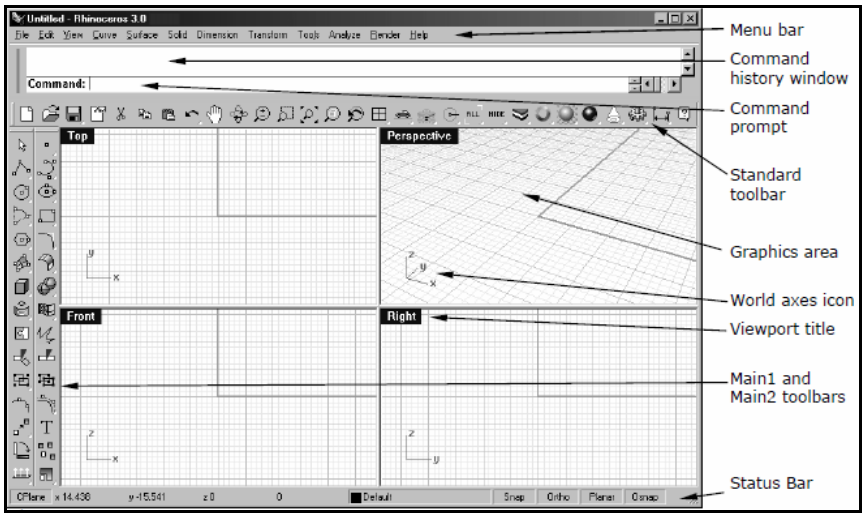

Figure 31. The Screen of Rhino Software (From: Ref. [26]).

Next, the model is saved as a 3ds format file. Urbana commands are then used to convert the 3ds file to a facet format file, and later, the edge format file is created. The facet and edge files will be added to the Urbana environment. Figure 32 shows Spanagel Hall created in Rhino. The dimensions of the building are 131.7 meters in length, 25 meters in width, and 30 meters in height. All materials are modeled as concrete, and windows, doors, and railings are not included in the model. The complex relative dielectric constant is:

$$\varepsilon_r = \varepsilon_r' - j\frac{\sigma}{\omega\varepsilon_\circ} = \varepsilon_r' - j\varepsilon_r'' \tag{4.1}$$

where:

σ = Conductivity of the material,

ε_r = Relative dielectric constant (real and imaginary),

ε_r' = Real component of the relative dielectric constant,

ε_r'' = Imaginary component of the relative dielectric constant, and

$\varepsilon_\circ$ = Free space dielectric constant.

For concrete the values are $\varepsilon_r' = 10.1$ and $\varepsilon_r'' = 0.5$, and thickness is set to be 0.3 m.

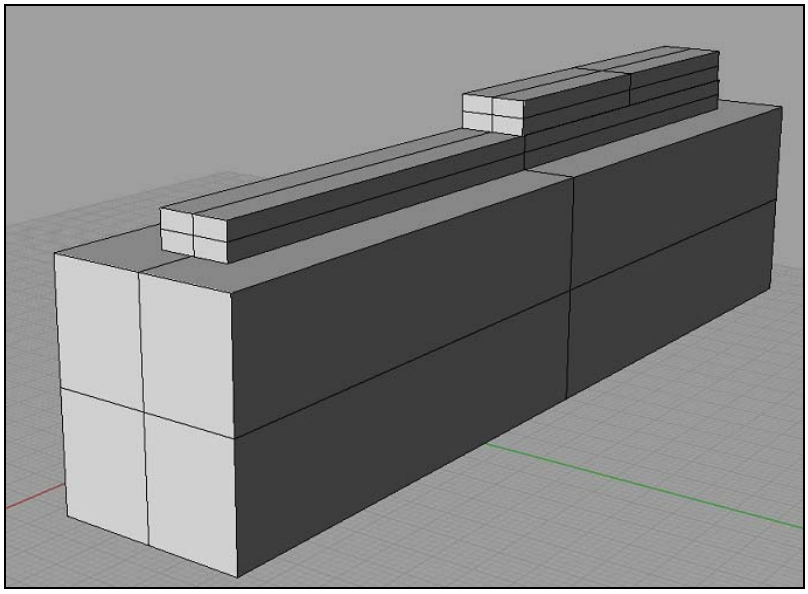

Figure 32. Spanagel Hall Created in Rhino Software.

The MICAz mote model was created in CST Microwave Studio as explained previously for the free space simulation. Figure 17 shows a picture of the model. The CST 3-D pattern file is saved and then imported into Urbana as an antenna type.

The process of creating the antenna file out of the MICAz mote model designed in CST Microwave Studio requires several steps. In CST Microwave Studio, a 3-D radio button is set on and the values for E-field are stored. From the Results menu, Plot Properties is selected, and then the Plot Mode tab is selected as seen in Figure 33.

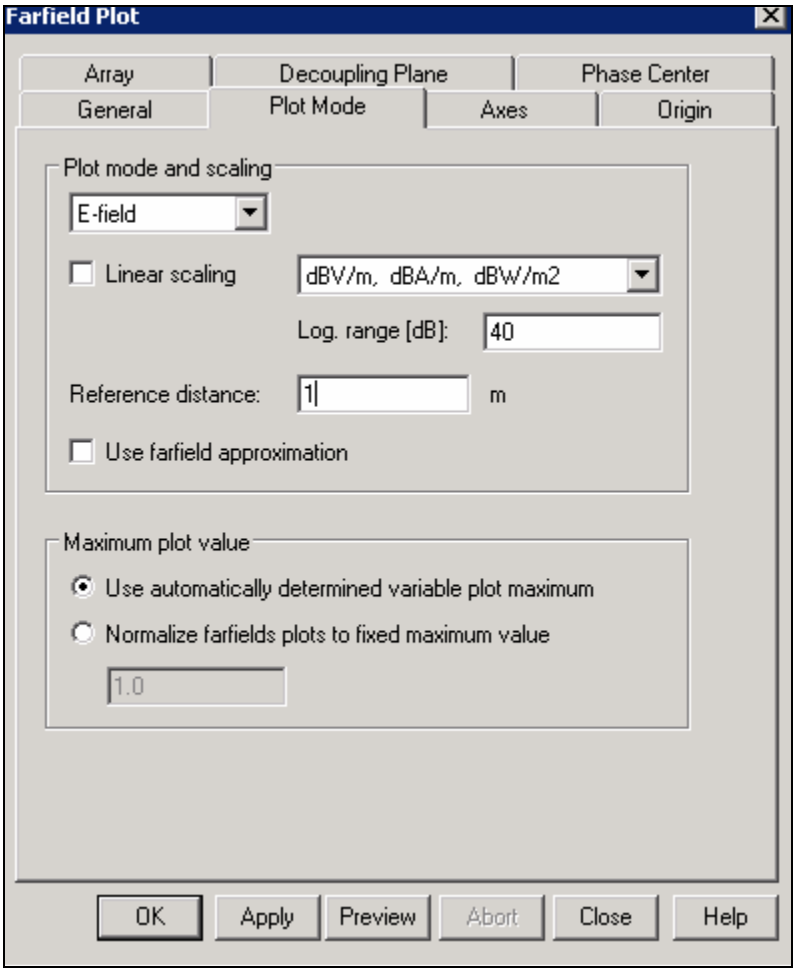

Figure 33. The E-Field Drop Down Menu in CST Microwave Studio.

These values of magnitude and phase are then exported to a text file as shown in Figure 34.

0.000	0.000	8.287e+000	8.131e+000	1.400	-6.637e+000	214.192	4.340e+000	6.024e+00
5.000	0.000	8.639e+000	8.503e+000	8.731	-6.967e+000	212.864	4.989e+000	6.160e+00
0.000	0.000	9.367e+000	9.260e+000	15.876	-7.383e+000	211.758	5.986e+000	6.673e+00
5.000	0.000	1.036e+001	1.028e+001	21.814	-7.879e+000	210.915	7.169e+000	7.503e+00
0.000	0.000	1.148e+001	1.142e+001	26.214	-8.447e+000	210.364	8.394e+000	8.520e+00
5.000	0.000	1.260e+001	1.256e+001	29.196	-9.081e+000	210.138	9.568e+000	9.591e+00
0.000	0.000	1.365e+001	1.362e+001	31.056	-9.772e+000	210.277	1.064e+001	1.062e+00
5.000	0.000	1.458e+001	1.456e+001	32.095	-1.051e+001	210.835	1.158e+001	1.156e+00
0.000	0.000	1.539e+001	1.538e+001	32.563	-1.127e+001	211.887	1.238e+001	1.237e+00
5.000	0.000	1.605e+001	1.605e+001	32.649	-1.204e+001	213.533	1.304e+001	1.305e+00
0.000	0.000	1.658e+001	1.657e+001	32.495	-1.280e+001	215.902	1.355e+001	1.359e+00
5.000	0.000	1.696e+001	1.696e+001	32.209	-1.352e+001	219.141	1.392e+001	1.398e+00
0.000	0.000	1.721e+001	1.720e+001	31.872	-1.416e+001	223.388	1.415e+001	1.424e+00

Figure 34. Data Exported into Text File from CST Microwave Studio.

The text file is manipulated by removing columns 1 to 3 and 8 to 9. Next, header lines are appended to the beginning of the antenna file as required by Urbana. Figure 35 depicts the file structure.

```
log_polar
theta_phi
vert_first
renorm
steps 36 72
   8.131          1.4        -6.637       214.192
   8.503        8.731        -6.967       212.864
    9.26       15.876        -7.383       211.758
   10.28       21.814        -7.879       210.915
   11.42       26.214        -8.447       210.364
   12.56       29.196        -9.081       210.138
   13.62       31.056        -9.772       210.277
   14.56       32.095        -10.51       210.835
   15.38       32.563        -11.27       211.887
   16.05       32.649        -12.04       213.533
   16.57       32.495         -12.8       215.902
   16.96       32.209        -13.52       219.141
    17.2       31.872        -14.16       223.388
   17.31       31.544        -14.68       228.726
   17.27       31.275        -15.04       235.118
```

Figure 35. The ANTPAT-Extension File with Header.

For patterns with cuts from 0˚ to 360˚, CST does not repeat the 0˚ cut at 360˚, so Urbana requires the addition of a 360˚ cut in the file shown in Figure 35. Rows 1 to 40 are copied and appended to the end of the file. The file is then opened using the MatLab file named "ReadAntennaFile.m" to plot and validate the antenna pattern. Finally, the file is added to the antenna library in the Urbana software.

These components are integrated together to start the measurements of the field around the mote. The location of the mote model with respect to the building is the same as in real measurements done on the roof of Spanagel Hall, which will make the results consistent. Figure 36 depicts the simulation components of the MICAz mote and Spanagel Hall in Urbana.

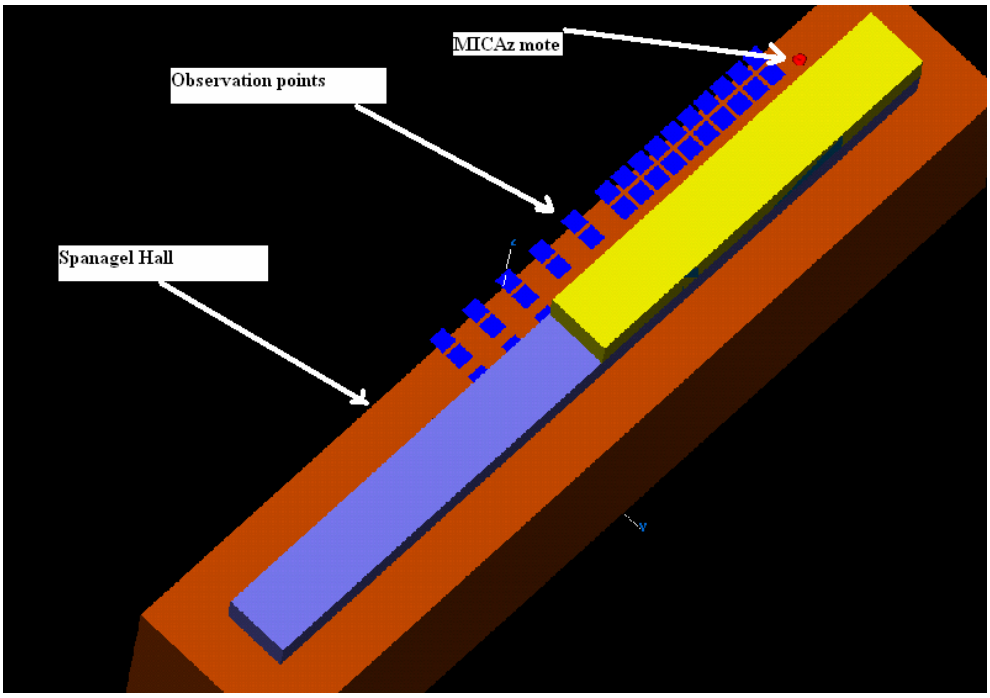

Figure 36. Components for the Simulation in Urbana.

1. First Configuration

The Urbana software requires observation points at which to calculate the electric field. These observation points are defined in a text file with their three-dimensional coordinates (*x,y,z*). The observation file is a set of points where the electromagnetic field is computed.

The measurement positions for the received power on the roof of Spanagel Hall were shown in Figure 26. These measurement positions are simulated as multiple observation points in Urbana. The file for the positions is prepared in a text file and then saved as an OBV extension.

The file is entered into the Urbana software under the Coverage Region tab and is used to calculate the received power. Figure 37 depicts the results of the simulation for the various observation points. The results of the received power distribution are subject to multipath. The observation points near the transmitter do not necessarily have higher power than those farther away due to constructive and destructive interference.

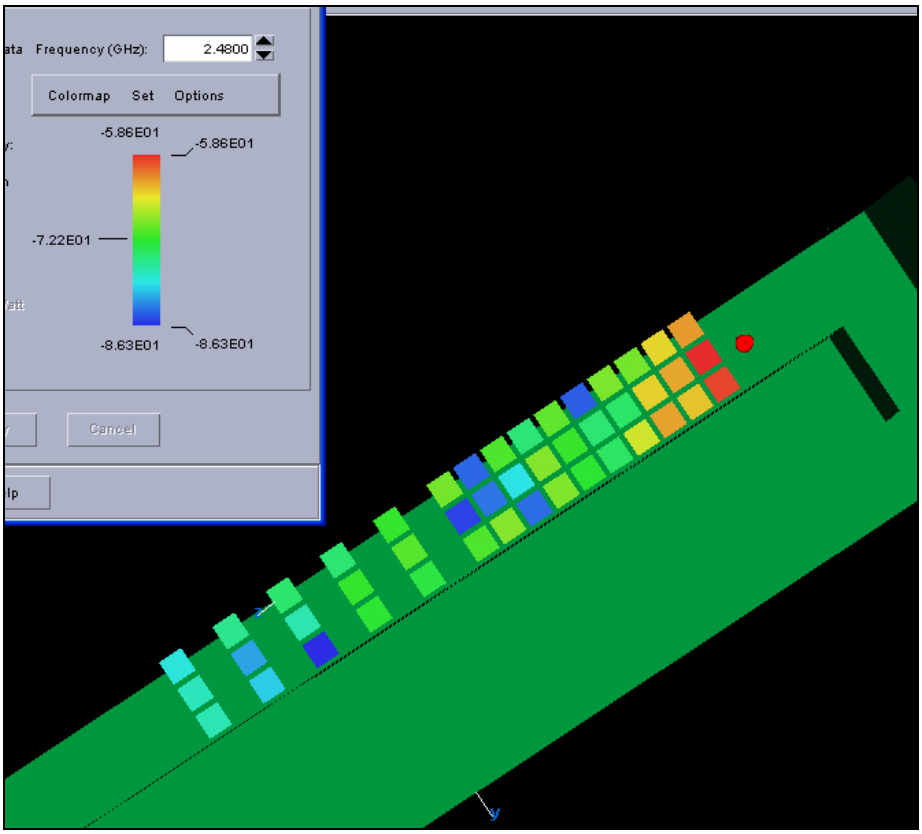

Figure 37. Results for the Simulation for Single Mote Running with Multiple Observation Points.

The Urbana software provides two types of outputs: an ASCII file and a contour plot. Figure 37 shows the color-coded graph output. The other type, which is the ASCII file, contains real and imaginary field components for the E-field. A MatLab code named "read_field_file.m" was used to convert the field values to power in dBm to compare with results measured in the experimental setup on the roof of Spanagel Hall. Figure 38 shows the graph of these converted results.

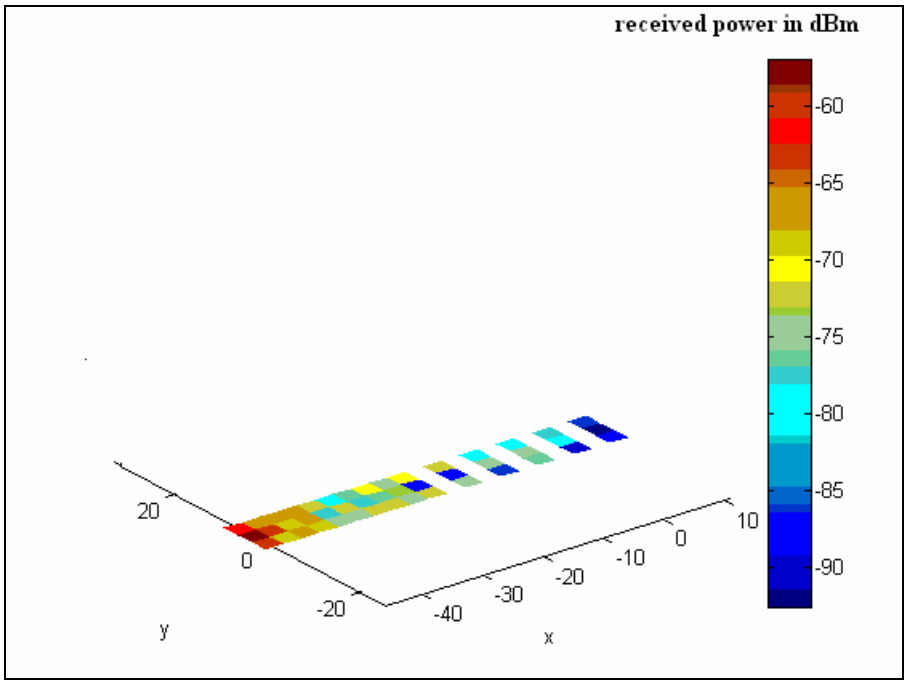

Figure 38. Results for the Simulation for Single Mote Running with Multiple Observation Points using MatLab Analysis Code.

There should be no difference between Figure 37 and Figure 38 if the color bars are identical. The results show that the distribution of power received correlates with the results of the experimental setup for the first measurement configuration, which indicates that the locations are experiencing the multipath effect. The relatively minor differences between the simulation and measurements are presented in Figure 39. These differences are within the measurement accuracy considering the differences in the measurement and simulation models. In real experimental setup, interference and harmonics occur due to other systems at the same frequency of operation. Another issue is the simple simulation model for the building is used; detailed features of the building and materials are neglected.

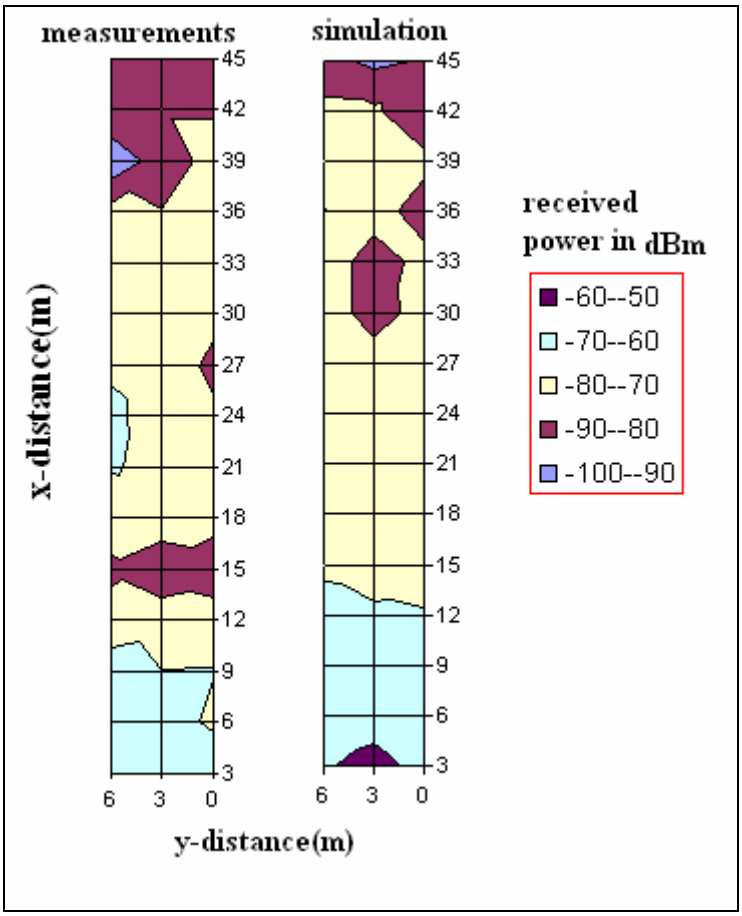

Figure 39. Comparison between Single Mote Real Measurement and the Simulation in Urbana.

2. Second Configuration

The human factor was added into the experimental setup in this case to validate the results from the measurements conducted in Chapter IV.C.2.

Several models could be used to simulate the effect of human presence between the transmitter and the receiver. The complex detailed model is available for the CST Microwave Studio as seen in Figure 40.a. The simplest model is the monolithic model of a human being as seen in Figure 40.b.

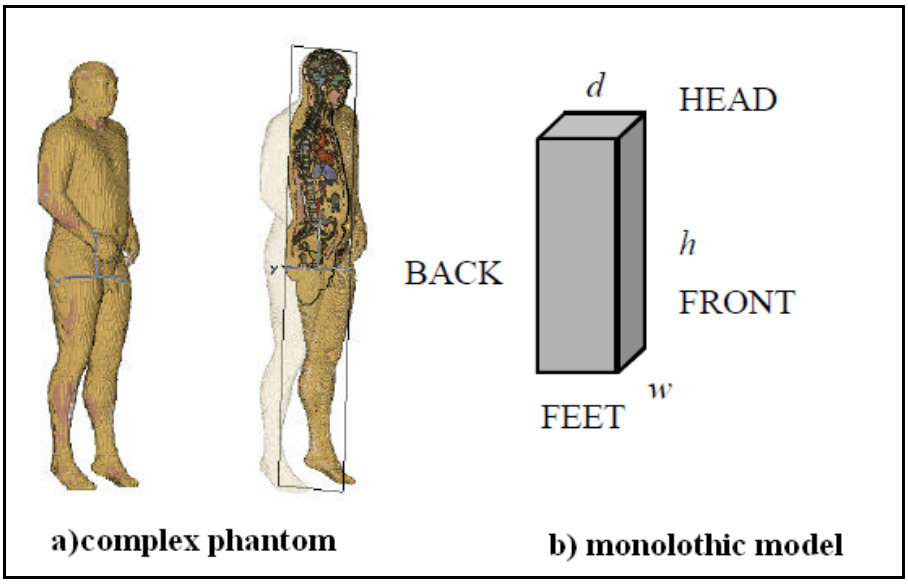

Figure 40. a) Complex Phantom. b) Monolithic Model. (From: Ref. [27]).

In this study, the simple model is used, which is the monolithic model. Dimensions for this model are a height *h* equal to 1.75 m (toe to head), width *w* equal to 0.45 m (across shoulders), depth *d* equal to 0.25 m (chest to back), in a volume of the body equal to $0.1969\,\mathrm{m}^3$. The average density of fat and muscle are equal to $\frac{1\mathrm{g}}{\mathrm{cm}^3}$, which provides a body mass of 92 kg.

The level of body absorption of wave energy and penetration into the body is determined by the conductivity (σ) and the real component of the relative dielectric constant (ε_r') of the body tissue as seen in Equation (4.1). These values are inserted into the Urbana software as the material characteristics of the monolithic model so that the simulation is complete. For muscle, $\sigma = 46\frac{\mathrm{S}}{\mathrm{m}}$ and $\varepsilon_r' = 2.3$, and for fat, $\sigma = 5.5\ \frac{\mathrm{S}}{\mathrm{m}}$ and $\varepsilon_r' = 1.5$. In this study, the values for ε_r' and ε_r'' are considered to be $\varepsilon_r' = 10$ and $\varepsilon_r'' = 0.7$ and thickness is set to be 0.25 m.

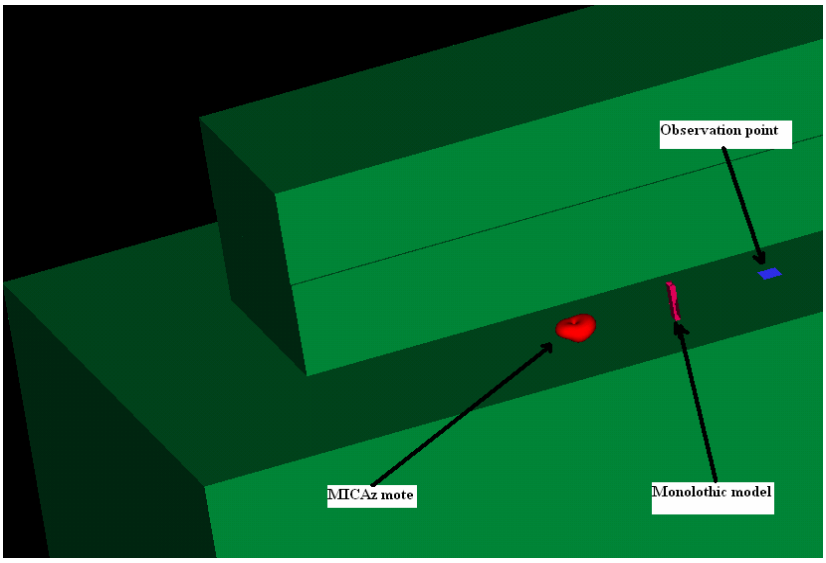

Figure 41. Simulation Set for Human Presence.

The simulation is run with the sequence elaborated in first simulation configuration in Chapter IV.D. The simulation steps are shown in Figure 42.a to 42.e. The positions of the human is moved from the transmitting mote location by 5 feet each time and the Urbana simulation software is run for each of those positions as shown in Figure 42.

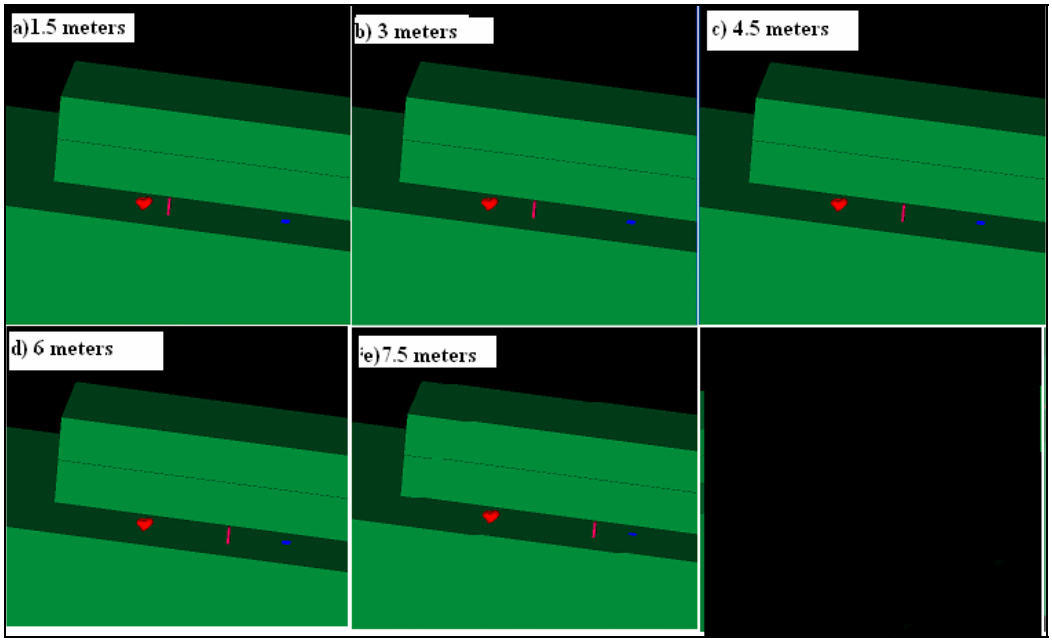

Figure 42. Simulations for the Human Presence at Different Distances between Transmitter and Receiver.

The results for this simulation model are shown in Figure 43. The effect appears to be low over all the distances, while the offset between the simulation results and measurement results is considerably high (as compared to Figure 29).

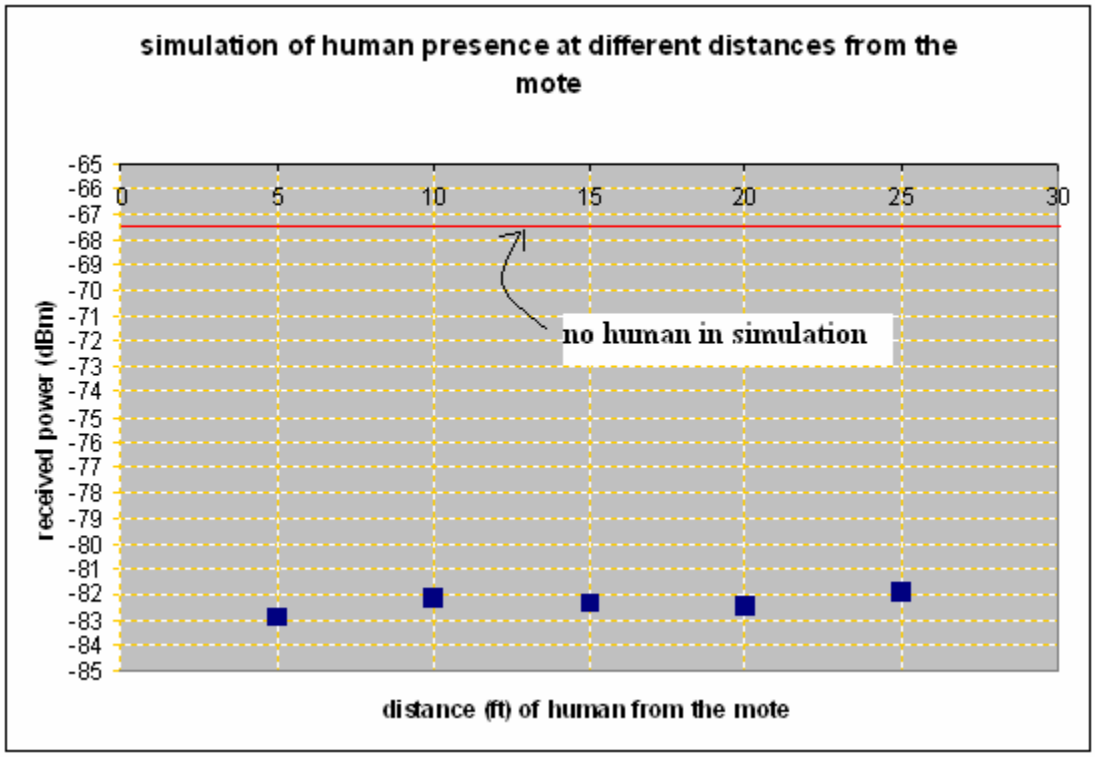

Figure 43. Results for the Simulation of the Mote with Human Presence at Different Positions with a Single Observation Points in Urbana.

3. Third Configuration

The third configuration of measurements previously discussed considers multiple MICAz motes in the experimental location. As discussed in Section IV.C.3, the transmission mechanism of the motes cannot be simulated with Urbana software.

Instead, those multiple sensors are assumed to be transmitting at the same time. This helps in understanding the power distribution around these motes, which makes the study of interference effect feasible. Figure 44 depicts the result of running the simulation of multiple motes in Urbana.

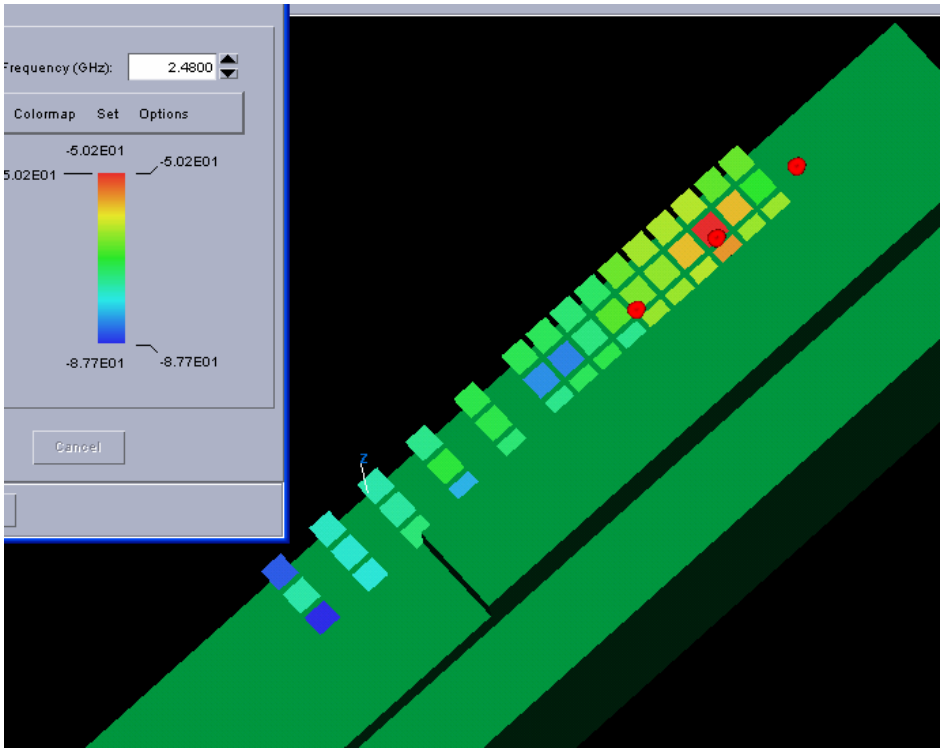

Figure 44. Results for the Multiple Mote Simulation Running with Multiple Observation Points in Urbana.

As stated previously, the assumption that those motes are transmitting at the same time is not really practical, since motes that transmit at the same time suffer data collisions. However this simulation was done to investigate the superposition and multipath effects. Three motes transmit simultaneously acting as a linear array. The received power at the observation points may be higher or lower due to the addition of power from multiple motes, depending on their relative phases and spacing.

The MatLab code named "read_field_file.m" was used to obtain Figures 45 and 46, which show the patterns when the excitation relative phase between the motes is $\pi/8$ and $\pi/4$, respectively. The motes are 3 m apart. Since the wavelength is $\lambda = 0.121\,\text{m}$, the spacing between the motes in wavelengths is $3/(0.121) = 24.8$. Taking out the integer number of wavelengths, the remaining relative phase due to spacing is (0.8) (360˚) =288˚. If the motes were to be used in this way, it would be important to control the phase to provide maximum radiation in the direction of the receiver.

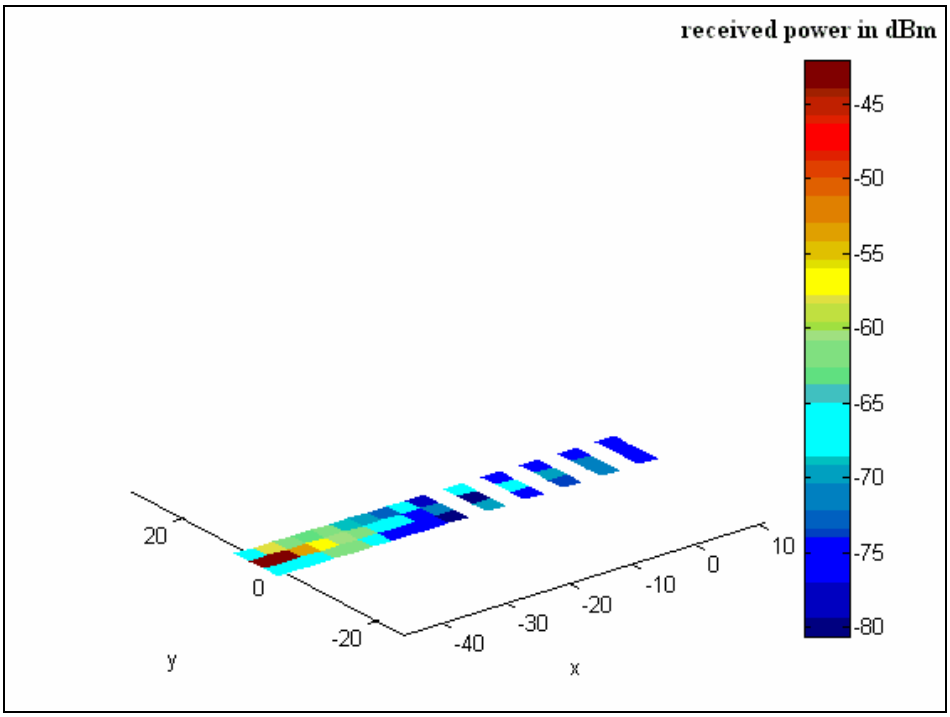

Figure 45. Results for the Multiple Mote Simulation Running with Multiple Observation Points in Urbana using MatLab Analysis Code (Phase 22.5°).

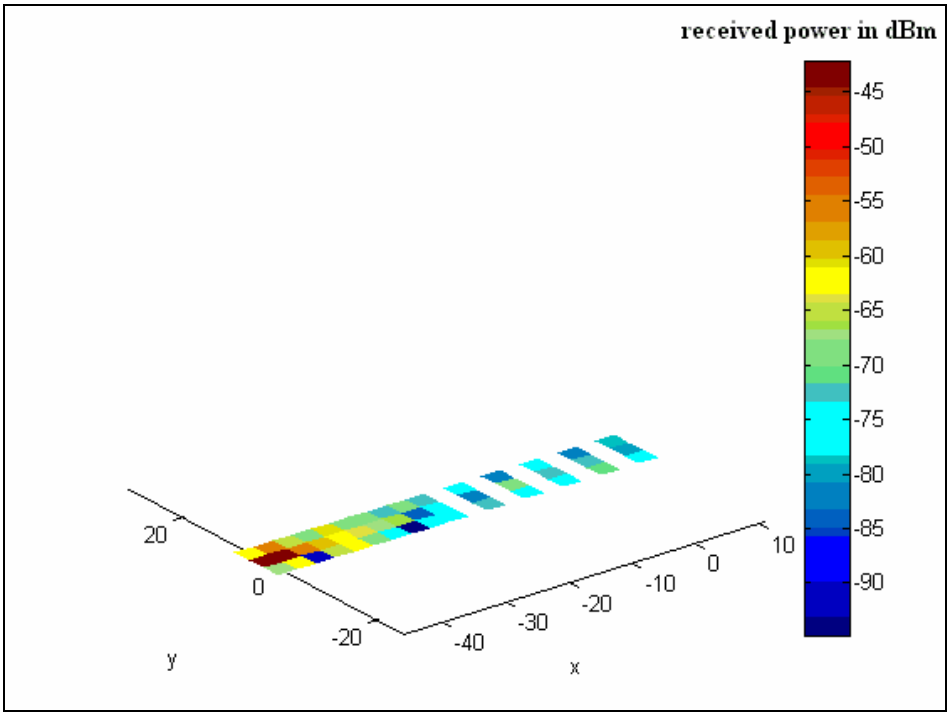

Figure 46. Results for the Multiple Mote Simulation Running with Multiple Observation Points in Urbana using MatLab Analysis Code (Phase 45°).

As shown in Figures 45 and 46, the comparison between the results clearly shows different power distribution using different phase between motes. Multipath effect with in-phase transmission is not as severe as when multiple motes transmit out-of-phase.

Comparing the results of single mote simulation shown in Figure 38 with the multiple motes simulation shown in Figure 46, it is clear that the power distribution is more uniform when multiple motes transmit at same time. Note that the phase difference between multiple motes plays a key role in determining the power received at the receiver. For example, the signal can be in-phase or out-of-phase causing signal enhancement or severe signal degradation.

E. SUMMARY

In this chapter, the experimental setup and data analysis of different measurements was conducted. Each experimental configuration was built in the Urbana simulator to validate the results gathered in the measurements. While some differences between the two are inevitable due to the difference between the simulation models and experimental setup, a considerable correlation was identified between the simulation and experimental measurements. In the next chapter, summary of the study results and recommendations for future work are presented.

V. SUMMARY AND RECOMMENDATIONS

A. RESULTS SUMMARY

The experimental setup and simulation model was built for the MICAz mote antenna. The main objective was to examine the effect of the pattern irregularity on the WSN systems. This section summarizes the experimental measurement and simulations results.

The MICAz mote radiation pattern was measured in a free space environment, i.e., the NPS anechoic chamber. The pattern irregularity was seen in the resulting measurements. These results were confirmed with the simulation for the same environment modeled in CST Microwave Studio.

The next step was to measure the radiation pattern for the MICAz mote in a multipath environment. The results showed the multipath effect, which results in non-uniform coverage of the transmitted and received radiation pattern around the mote. The simulation performed in the Urbana software confirmed the same results.

Although the irregularity is due to the channel characteristics, it effectively changes the radiation pattern of the mote. The irregularity of the radiation pattern of the mote itself in free space was shown in Chapter IV.A. There are several notches or "dips" in the pattern due to the antenna being mounted asymmetrically on the mote body. The pattern is modified further when the mote is set on the ground and introduced into a multipath environment.

Another addition to the experimental setup was a human presence between the transmitter and the receiving system to study the effect on the received power. The monolithic model for the human being was created in Rhino and then added to the same platform created earlier in Urbana. The simulation results correlated with the results from the experimental setup.

It was clear that the effect of the human presence was considerable when the human being was near the transmitter or the receiver where blockage occurs. The effect is negligible in the middle area between the transmitter and the receiver.

The last portion of the experimental setup was adding multiple motes. Due to the transmission mechanism of the MICAz motes, the measurement of the effect of multiple motes was not feasible. Simulation was the solution to this problem with the assumption that all motes transmit at the same time.

Studying the multiple motes case would provide information about coverage in the presence of the multipath for the case of multiple motes transmitting. However, this is not in the normal transmission mechanism, which is one mote sends while the other motes listen.

The results from the experiment and simulation are useful for the implementation and design of WSN systems. The propagation characteristics should be accounted for in the design and implementation of the network to satisfy the criteria of topology, connectivity, deployment, and coverage.

1. Topology and Connectivity

The connectivity in the WSN depends on the transmitted and received power level. The received power level must be higher than a specific threshold in order to establish a connection. The topology of the WSN is the key element that determines the manner in which the WSN is connected together, and it is also dictated by the connectivity of the sensor nodes. If the transmit power is uniformly distributed around the mote, the sensor placement and coverage area would be determined easily. In this thesis, the irregularity of the range around the mote is shown to be significant, thus, making it evident that one should design networks with the irregularity in mind.

2. Deployment and Coverage

The deployment of the motes in the field is affected by the radiation pattern of the motes. Several approaches could be taken to study this problem so that placement guideline can be established. One approach is modeling different environments, such as vegetation, forest, urban area, desert, a small city or a large city a similar is taken in modeling indoor and urban propagation.

Using the information about the received power distribution, the probability of nodes connecting with each other could be used to minimize the number of motes needed to cover a specific area.

B. RECOMMENDATIONS AND FUTURE WORK

This thesis is a building block of continuous research in the area of WSN. Further study of sensor radiation pattern and its impact on sensor placement, simulating the whole sensor network in Urbana, investigate coverage protocol with the given patterns, and thorough study of human affect on received power is highly recommended. While MICAz motes have been used in the experimental setup, the use of other wireless sensor node vendor products will make the current results more generally applicable.

THIS PAGE INTENTIONALLY LEFT BLANK

LIST OF REFERENCES

[1] Zhou, Gang, He, Tian, Krishnamurthy, Sudha and Stankovic, John A., "Impact of Radio Irregularity on Wireless Sensor Networks," *MobiSYS 2004,* June 6-9, 2004, Boston, Massachusetts, USA.

[2] Kotz, David, Newport, Calvin and Elliott, Chip, "The Mistaken Axioms of Wireless-Network Research," Dartmouth College Computer Science Technical Report TR2003-467, July 18, 2003.

[3] Zhon, Zongheng, Das, Samir and Gupta, Himanshu, "Variable Radii Connected Sensor Cover in Sensor Networks," *Sensor and Ad Hoc Communications and Networks 2004. IEEE SECON 2004*, Page(s):387 – 396, Santa Clara, California, USA, Digital Object Identifier 10.1109/SAHCN.2004.1381940.

[4] Tingle, Mark E., "Performance Evaluation of a Prototyped Wireless Ground Sensor Networks," Master's Thesis, Naval Postgraduate School, Monterey, California, March 2005.

[5] Swee, Jin Koh, "RF Characteristics of MICAz Wireless Sensor Network Motes," Master's Thesis, Naval Postgraduate School, Monterey, California, December 2005.

[6] Gupta, P. and Kumar, P. R., "Critical Power for Asymptotic Connectivity in Wireless Networks," in Stochastic Analysis, Control, Optimization and Applications: A Volume in Honor of W. H. Fleming, W. M. McEneany, G. Yin, and Q. Zhang, Eds. Boston, Massachusetts: Birkhauser, 1998, pp. 547–566.

[7] Sanchez, M., Manzoni, P. and Haas, Z. J., "Determination of Critical Transmission Range in Ad Hoc Networks," in Multiaccess Mobility and Teletraffic for Wireless Communications 1999 Workshop, October 1999.

[8] Xue, Feng and Kumar, P. R., "The Number of Neighbors Needed for Connectivity of Wireless Networks," *Wireless Networks*, Vol. 10, pp. 169-181, 2004.

[9] Kleinrock, L. and Silvester, J., "Optimum Transmission Radii for Packet Radio Networks or Why Six is a Magic Number," *Proceedings of National Telecommunications Conference*, Birmingham, Alabama, December 1978, pp. 4.3.2-4.3.5.

[10] Takagi, H. and Kleinrock, L., "Optimal Transmission Ranges for Randomly Distributed Packet Radio Terminals," *IEEE Transactions on Communications*, Vol. COM-32, No. 3, pp. 246-257, March 1984.

[11] Royer, E.M., Melliar-Smith, P.M. and Moser, L.E., "An Analysis of the Optimum Node Density for Ad Hoc Mobile Networks," *Proc. International Conference on Communications 2001*. Volume 3, 11-14 June 2001, Page(s):857 - 861 vol. 3, June 11-15, 2OO1, Helsinki, Finland.

[12] Li, L., Bahl, V., Wang, Y.M. and Wattenhofer, R., "Distributed Topology Control for Power Efficient Operation in Multihop Wireless Ad-Hoc Networks," *Proc. IEEE INFOCOM 2001*, Volume 3, 22-26 April 2001, Page(s):1388 - 1397 vol.3. INFOCOM 2001: Anchorage, Alaska, USA.

[13] Xiao, Li and Xu, Zhichen, "On Energy Efficiency and Network Connectivity of Mobile Ad Hoc Networks." *Proc. of ICDCS 2003*, Providence, Rhode Island, USA, May 2003. 19-22 May 2003 Page(s):38 – 45.

[14] Stuedi, Patrick, Chinellato, Oscar and Alonso, Gustavo, "Connectivity in the Presence of Shadowing in 802.11 Ad Hoc Networks," *IEEE Communications Society / WCNC 2005.* Volume 4, 13-17 March 2005 Page(s):2225 - 2230 Vol. 4, New Orleans, Louisiana, USA.

[15] Z´u˜niga Z., Marco and Krishnamachari, Bhaskar, "Optimal Transmission Radius for Flooding in Large Scale Sensor Networks," Department of Electrical Engineering, University of Southern California, Los Angeles, California, 90089, USA.

[16] Akyildiz, W. Su, Sankarasubramaniam, Y. and Cayirci, E., Wireless sensor networks: A Survey, I.F., Broadband and Wireless Networking Laboratory, School of Electrical and Computer Engineering, Georgia Institute of Technology, Atlanta, Georgia, December 2001.

[17] Murthy, C. and Manoj, B. S., Ad Hoc Wireless Networks Architectures and Protocols, pp. 647-693, Prentice Hall, Upper Saddle River, New Jersey, 2004.

[18] Heinzelman, W., Chadrakasan, A. and Balakrishnan, H., "Energy-Efficient Communication Protocol for Wireless Microsensor Networks," *Proc. of Hawaii International Conference on System Sciences 2000*, pp. 4-7, Hawaii, USA, January 2000.

[19] Ding, Jin, Kashyapa, Sivalingam K. and Chuan, Lu Jian, "A Multi-Layered Architecture and Protocols for Large-Scale Wireless Sensor Networks," *Proc. of Vehicular Technology Conference 2003*, VTC 2003-Fall, 6-9 October 2003, Orlando, Florida, USA, IEEE 58th, Volume 3, pp. 1443-1447.

[20] Urbana User Manual, Science Applications International Corporation (SAIC), 2003. Available at http://www.saic.com/products/software/urbana/, last accessed May 2006.

[21] Wong, K. Daniel, "Physical Layer Considerations for Wireless Sensor Networks," IEEE International Conference on Networking, Sensing & Control, Taipei, Taiwan, March 21-23, 2004. Volume 2, 2004 Page(s):1201 - 1206 Vol. 2, Digital Object Identifier 10.1109/ICNSC.2004.1297118.

[22] Callaway, Edgar H., Jr. *Wireless Sensor Networks, Architecture and Protocols*, Boca Raton, Florida. Auerba Publications, CRC Press, c2003.

[23] Rappaport, T. S., *Wireless Communications Principles and Practice*, pp. 105-253, Prentice Hall, Upper Saddle River, New Jersey, Second Edition.

[24] Technical Staff Crossbow Technologies Inc MPR/ MIB User's Manual," Rev. B, April 2005, Document Part No. 7430-0021-06, Crossbow Technologies Inc., San Jose, California, USA, 2005, http://www.xbow.com/Products/Product_pdf_files/Wireless_pdf/MICAz_Datasheet.pdf, last accessed January 2006.

[25] Erenoglu, Burcak, "Naval Postgraduate School Anechoic Chamber Evaluation," Master's Thesis, Naval Postgraduate School, Monterey, September 2004.

[26] Rhinoceros Training Manual v3.0, Robert McNeel & Associates 2005. Available at http://www2.rhino3d.com/resources/default.asp?show=Book&search=&language=en, last accessed May 2006.

[27] Jenn, D. C., Lecture Notes for EC3630, Radio Wave Propagation, available at www.nps.navy.mil/jenn/EC3630list.html, last accessed May 2006.

THIS PAGE INTENTIONALLY LEFT BLANK

INITIAL DISTRIBUTION LIST

1. Defense Technical Information Center
   Ft. Belvoir, Virginia

2. Dudley Knox Library
   Naval Postgraduate School
   Monterey, California

3. Chairman, Code EC
   Department of Electrical and Computer Engineering
   Naval Postgraduate School
   Monterey, California

4. Professor Weilian Su
   Department of Electrical and Computer Engineering
   Naval Postgraduate School
   Monterey, California

5. Professor David Jenn, code EC/Jn
   Department of Electrical and Computer Engineering
   Naval Postgraduate School
   Monterey, California

6. Mr. Bob Broadston
   Naval Postgraduate School
   Monterey, California